Application of Cutting-Edge 3D Seismic Attribute Technology to the Assessment of Geological Reservoirs for CO_2 Sequestration

Type of Report: Progress

Frequency of Report: Quarterly

Reporting Period: April 1, 2009 – June 30, 2009

DOE Award Number: DE-FG26-06NT42734 [University Coal Research]
(UH budget G091836)

Submitting Organizations: Department of Earth and Atmospheric Sciences
Reservoir Quantification Lab
University of Houston
Houston, Texas 77204-5505

Preparers: Prof. Christopher Liner - P.I.
Dr. Jianjun (June) Zeng
Dr. Po Geng
Heather King
Phone: 713-743-919
Fax: 713-748-7906

CONTENTS

Executive Summary

This report presents major advances in progress made through the report period from March 1 to June 30 of 2009 for the Dickman Field CO_2 sequestration project. First, accurate depth-conversion of seismic amplitude and attribute volumes has been accomplished by correction of time-depth misties in the third-generation earth model (M3). Fault and fracture interpretations have been reconciled from an integrated study of seismic volumetric attributes and geological data. Third, lithology correction of zone-averaged neutron porosity log data has been completed allowing estimation of permeability for export to the Computer Modeling Group flow simulation software. Fourth, we have corrected mismatches of zone-averaged rock properties for partially penetrated litho-zones. Finally, we show initial results of flow simulation and history matching for the Dickman field shallow reservoirs.

Activities in Quarter

Geology and Geophysics

Significant improvements for the geological integrity of the third-generation earth model (M3) model have been achieved. After revising velocities based on five zone-averaged five sonic logs in the survey area, the depth-converted structural framework from seismic interpretation resulted in a new M3 depth model with reasonable precision when compared to the gridded surface from raw well top data. For example, the Fort Scott Limestone Formation (often used as a hanging datum) now has +/- 2 ft error inside the 3D survey area, the Miss. Unconformity (boundary separating Lower Cherokee Sandstone and Miss. cherty dolomite reservoirs) is +/- 6 ft error, and the Gilmore City Unconformity (base of saline aquifer) is +/- 12 ft error. These boundaries were used by the CMG simulator for the history matching process.

This revised velocity model allows the depth-conversion of all seismic attribute volumes, including volumetric geometry attributes such as variance, chaos, dip, azimuth, positive and negative curvatures, impedance, and ANT Volumes. The volumetric geometry attribute volumes therefore can be used to evaluate the inter- and confined linear and non-linear features within the target geological window with true subsurface geometry. These features may be attributed to structural deformation or karst-related dissolution for corresponding stratigraphic units.

For the litho-correction of zone-averaged neutron porosity in property modeling, linear relationships were defined and used because the auto-correction tool is not available in Petrel. Correction functions were drawn by sampling from ideal litho-correction curves on the neutron porosity v. density cross plots with the porosity values ranging from 0 to 40%. The corrected porosity was used to estimate the permeability for the shallower reservoirs, based on the relationship drawn from the core porosity and core permeability measurements from 7 wells. For the property modeling of the deep saline aquifer with limited penetration, the depth-converted seismic impedance volume is used to assist the propagation of reservoir porosity and permeability.

The last planned task, the correction of mismatches between zone property and litho-zone names in partially penetrated zones, was performed on only a limited number

of key wells instead of a global-correction for all partial-penetration wells. Wells are corrected by using the zones as filters to control reservoir property distribution. This avoids using a global correction that would result in thickness errors since partially - penetrated litho-zones would be mistakenly replaced by their penetrated thickness. An alternate approach is to assign property values to grid cells using the "up-scaling logs" process through penetrated thickness of litho-zones. for a disadvantage to this approach is the difficulty in zone-by-zone litho-correction of porosity logs. Both approaches significantly reduce the workload on hand-correction of zones well-by-well. The following three sections present in detail the steps for and results from these tasks and the expected risks remaining for the flow simulation.

Depth-conversion of M3 Model and Seismic Attribute Volumes

The major improvement of time-depth conversion for the M3 model came from the correction of interval velocities as the input to construct the velocity model. In the 3D survey area, only three wells contain sonic logs (Dickman 1, Dickman 6 and Elmore 3 in the north and central areas of the survey, Fig. 1-1). Two wells containing both sonic and density logs are outside the seismic boundary (Humphrey 4-18 to the west, and SideBottom 6 to the southeast of the survey). These wells were projected to the nearest seismic traces so that five wells became available, meeting the minimum requirement for interpolating or extrapolating the interval velocity from five points through the entire survey area.

To re-compute the interval velocity from the five sonic logs, we corrected mismatches between computed interval-velocity and the corresponding litho-zones (caused by a tool defect) by adding pseudo-tops representing partially penetrated or missing zones in five wells. This enables each partial- or non-penetrated zone to have a pseudo zone name with a penetrated or zero thickness registered in the database. The zone-averaged sonic values are computed over this depth range as the interval velocity Validation was done zone-by-zone for the interval velocity results Excel. Interval velocities were converted from feet/sec to meter/sec, edited to eliminate extreme values, and gridded to create interval velocity surfaces (Fig. 1-2a-e). The figures show interval velocity surfaces gridded from five data points (maps to the left of each figure) and the

distribution of interval velocity values in the grids (histograms to the right of each figure). From the histograms, the velocity peak value for each shallower litho-zone is significant: Over 50% of the values range from 3950 to 4060 m/sec for Fort Scott Limestone, from 3920-4040 m/sec for Lower Cherokee, and from 4550-4650 m/sec for Mississippian. The interval velocity distribution for the deeper litho-zones is based on only 2 points, with over 50% of the values at 4648 m/sec for Osage and no peak value for the Gilmore City. The gridded velocity maps show systematic anomalies resulting in significant spatial variations (about 1000 m/sec) in interval velocity. Taking Fort Scott Limestone as an example, interval velocity computed from the Dickman 1 sonic is 10% higher than that computed from the nearby Dickman 6 sonic, and 8% higher than that computed in the Sidebottom 6. The lateral variations of interval velocities exist for all intervals, caused by the generally higher values in SideBottom 6 well. This is very likely due to differences in measurement environment for logging, rather than the lateral variation of acoustic properties of limestone strata. Since complete data for original environment conditions are not available and Petrel has no environment correction tools for logs, the 5-7% extreme highs and 5-7% extreme lows of interval velocity values for surfaces in Fig. 1-2 were removed from the input data in building the velocity model. The velocity model takes input from "interval velocity surfaces" using about 85% of values around the peak distributions. The resulting depth surfaces are corrected by more than 20-30 time-depth pairs at wells for the shallower reservoir zones and 3 time-depth pairs at wells for the deep saline aquifer zones. These time-depth pairs were determined by seismic study using SMT Kingdom software reported in the March 31, 2009 report.

The depth-converted M3 model using improved velocity shows acceptable precision, as validated by comparing the depth-converted framework to well top data. Fig. 1-3 shows the differences between the two superimposed surfaces for Fort Scott, Mississippian Unconformity, Osage Mississippian dolomite saline aquifer, and Gilmore City (Fig.1-3a-d). A vertical exaggeration of 5:1 is used in all maps to highlight differences between the two maps. Except the far north and far west areas (the areas with no velocity control available and having the influence of the north boundary fault), errors between the two tops are < 2 ft for Fort Scott Limestone (hanging datum of the structural model), <6 ft for the Mississippian Unconformity (separating the LCK sandstone above

and the carbonates below), <6 ft for the Osage Mississippan dolomite (surface defining the saline aquifer), and < 12 ft for the Gilmore City (base of simulation grid). This improved M3 stratigraphic framework serves as initial input for history matching for CMG flow simulation. Moreover, the comparison in Fig. 1-3 indicates that the improved velocity model is good enough to allow the depth-conversion of all computed seismic attribute volumes, including passive and aggressive ANTs, positive and negative curvatures, dip, azimuth, coherence and chaos for geological interpretation of the fault/fracture framework, as well as the impedance volume for property modeling of the deep saline aquifer.

Study of Fractures Revealed by Depth-converted Seismic Attributes

A major goal of this project is using cutting-edge technology in volumetric seismic attributes to assist the understanding of the fault and fracture framework. Volumetric seismic attributes have several advantages over conventional horizon seismic attributes. These include labor savings since no horizon picking is needed, avoiding interpreter bias in defining features, and reducing systematic errors for merged surveys (Marfurt, 2009). However, features obtained from volumetric attributes are influenced by depth geometry and properties of overlying strata. After being computed, they should be viewed in depth and to scale to determine their geological reasonableness and implications. For instance, fault surface slopes on time sections can be very misleading, but after depth conversion associate with geological dip. Moreover, linear or non-linear features revealed by seismic geometry attributes are best interpreted as structural, sedimentological or geomorphological features when depth converted and tuned by roughly matching vertical analysis window size to the target thickness.

In this study, it is especially important to obtain seismic attribute and impedance volumes in true geological scale for the quantitative flow simulation of deep saline aquifer. Data extracted from the seismic attribute study will serve as a major source of input for the simulation due to sparse well coverage relative to seismic common midpoint locations. If interpretation of seismic attributes can be validated by geology of the shallower reservoir targets, the same interpretations can be extended with confidence to the deep saline aquifer which is penetrated by only two wells. The volumetric attributes

that will be discussed and illustrated in the following sections are all depth-converted to reveal their true sub-surface geometry.

The effective interpretation of linear or non-linear features revealed by seismic geometry attributes must be based on the understanding of stratigraphic and structural details. As reported in the Mar. 31, 2009 Quarterly report, both unconfined and confined structural features exist in the target carbonate zone, as described in the Upper Osage reservoir of the nearby Schaben Field (Franseen, et. al., 1998; Franseen, 2006) and shown by 3D theoretical carbonate deformation models (OuYang, 1994). These features affect the reservoir fluid conductivity at varying levels. The unconfined features are mostly faults and joints penetrating the entire target interval due to brittle structural deformation. They form regional conduits or barriers for the flow in the flow simulation processes. The confined features are limited to certain carbonate zones and are most likely due to dissolution along areas or planes of weakness, including dissolution-prone depositional facies, fractures and faults. Confined features can also be formed by pressure dissolution associated with structural deformation either parallel or perpendicular to bedding planes, but mostly within specific layers (Fig. 8 of March 31, 2009 report). All the above confined features can serve as guidance to propagate porosity and permeability within the strata to feed flow simulation grids.

Karst topography developed at an unconformity surface may inherit features developed at an older, deeper unconformity if brittle deformation is operating. As a result, superimposed confined features can merge into apparent unconfined ones useful for tracing faults in the structure framework. For instance, some sinkhole geometry occurring below the Gilmore City unconformity was inherited to form channels at the Mississippian unconformity level, as will be detailed in the following sections.

Seismic geometry attributes have variable resolving power to visualize these unconfined or confined features. Fig. 1-4 shows selected depth-converted geometry attribute volumes displayed with vertical exaggeration of 10:1 to enhance visualization of features and vertical connections. Although all seismic geometry attributes are useful, the ANT volumes, especially the ANT Aggressive volume (Fig. 1-4a), best show the unconfined features for extracting faults and joint planes for the specific target strata in the Dickman field. This will be detailed in the next section. On the other hand, the chaos

and variance volumes visualize confined features better than unconfined ones (Fig. 1-4c to d). Their lateral variations are more significant at slices near the Mississippian and Gilmore City unconformity surfaces, as will be detailed in the next section. The two curvature volumes (Fig. 1-4b) originally loaded from GeoFrame seem to be of intermediate use for visualizing confined and unconfined features, regardless of the vertical window length and lambda parameters. The confined features illustrated by curvature volumes may be related to apparent unconfined structure such as inherited karst topographies. The local dip and azimuth volumes do not show significant lateral or vertical continuity (Fig. 1-4e and f). They can be used with other volumes to further study specific features.

ANT attributes and faults/joints

Two ANT seismic volumes using passive and aggressive methods were created from one structurally-smoothed, edge-enhanced coherence volume. In the process, a tool called "Ant agent" traces cells in all directions to connect cells with strong edge signals. "Passive" Ant-tracking, useful for visualizing major regional fault zones, requires stronger signals to advance further in the volume. "Aggressive" Ant-tracking detects subtle connections to reveal secondary or subtle fault/joint zones. Figures 1-5a and 1-5b show linear features traced by passive and aggressive ANT settings, respectively. Several linear features overlay fault segments hand-picked on seismic lines.

Following ANT tracking is a plane-extraction process resulting in a collection of surface segments with different areas, dip angles, azimuths, and level of confidence of connectedness. In the survey area, 217 and 262 planes were extracted from the passive and aggressive ANT volumes, respectively. Of all extracted ANT planes, over 80% from Passive ANT and 90% from Aggressive ANT are less than 30° in dips while less than 10% have dips greater than 60°. Attributes of some example planes are shown in Table 1. Selected planes for possible geological interpretation are shown in Figs. 1-6a-b at 1:1 scale with the Oil Water Contact (OWC) surface together and well locations as spatial reference. The part of each fault plane beneath the OWC is shaded by the OWC but is still visible. The selection of planes displayed in Fig. 1-6 is based on the following five criteria: (1) dips > 5° to exclue possible bedding planes and data errors, (2) azimuth not

parallel to the inline or cross direction to eliminate acquisition footprint and survey boundary edge effects, (3) a penetration interval from -1400 to -2400 ft TVDSS and cutting through the OWC (-1981 ft TVDSS) thus affecting target reservoirs and saline aquifer, (4) a surface area cutting more than 2000 grid cells to eliminate minor features that may noise-related, and (5) a confidence factor greater than 15 indicating higher degree of plane connectedness. Features passing this criteria screen are likely to be faults or major joints due to brittle deformation of the strata.

Among selected planes only two have dips greater than 60°, as shown in Fig. 1-7a. One is NE-oriented (N48°E), dip angle of 76° to NW, and is about 2000 ft long within the survey area. It is the north boundary normal fault causing significant displacement of strata (down-thrown on the NW side). This fault is clearly visible in the seismic amplitude data. The other plane in Fig. 1-7a is SE-oriented (S130°E), dip angle of 60° to NE, and is about 6000 ft long within the survey area. It does not coincide with any feature visible in other attributes (Fig. 1-5) and will be re-evaluated in the seismic amplitude volume to determine validity. The strike-extension of both planes is outside the survey boundary.

In Kansas, major pre-Desmoinesian post-Mississippian structural elements exhibit two structural trends (azimuth 20° and 315°) roughly perpendicular and parallel to the axis of the Central Kansas Uplift (CKU), respectively. True NE-oriented faults are rare (Merriam, 1963). The North Boundary Fault is much younger and does not belong to either catagory. It was active through Fort Scott time (Upper Desmoinesian). The SE-oriented one shown in Fig. 1-7a is roughly parallel to the axis of the CKU, and becomes obscure above the Fort Scott Limestone datum. Its origin could be related to post-Mississippian activity of the CKU that ceased after formation of the Fort Scott Limestone. Fig. 1-7b shows planes with dips greater than 45°. Three more NW-oriented planes are observed along with the one > 60° shown in Fig. 1-7a. Unlike the North Boundary Fault detected by both passive and aggressive ANT volumes, all the high-angle NW planes are seen only in the aggressive ANT volume. This indicates that the geometry of NW-oriented high angle planes is more subtle than that of the NE-oriented North Boundary Fault. Fig. 1-7c and 1-7d show planes with dips between 30-45° and 15-30°, respectively. The very low angle planes (15-30° dip) were extracted from the aggressive ANT volume

only. Whether they are faults or joints needs to be further studied, because only a few correlate to hand-picked faults with visible vertical displacements. Previous study on fifth-order structures in Kansas reveals three azimuth trends: 12° , 40°, and 320°. Carbonate joints (breakage with no displacement) are normally at 55° (Merriam, 1963). The planes we observe mostly fall within the 40° and 320° categories while almost none fall along 12° azimuth.

Several questions about the ANT study must be answered for a complete structural interpretation. Since the North Boundary Fault and associated fractures/joints are younger than Fort Scott time, is important to determine if these features are open or closed (in a fluid conductivity sense) for evaluation of CO_2 sequestration seal quality. A previous curvature study suggested that NE-oriented fractures are closed, acting as flow barriers (Nissen et. al., 2006). The major North Boundary Fault is currently taken as an up-dip seal for the Dickman Field in the CMG flow simulator. However, a normal fault formed under extensional force was unlikely a closed one at the time of formation. Fractures parallel to the North Boundary Fault, if formed under the same stress field, should also be open at the time of origin. They were likely planes of weakness and prone to carbonate dissolution, perhaps slightly disrupting seismic data and making them detectable by passive ANT tracking. If they are considered as a flow barrier, then there should be post-formation processes that altered them from open to closed. Further study is required.

In addition to the first–order structure related to CKU in the survey area, we have observed a secondary north-east plunging anticline roughly perpendicular to the axis of the CKU (see Fig. 5 and 7 of March 31, 2009 Quarterly report). The North Boundary Fault is parallel to the axis of this secondary anticline and compressional stress related to its formation is a possible cause for the NE Fault/fracture/joint set close, making it an up-dip seal. However, this interpretation requires correct timing between the fault closure and trap formation. However, according to the theoretical carbonate deformation model (Fig. 8 of March 31, 2009 report), if these fractures were formed with the secondary NE-plunging anticline, they could be open extensional fractures. In this case, they would become a concern for CO_2 sequestration seal integrity. However, they should theoretically be nearly vertical, rather then at very low angles indicated by ANT tracking

(5° to 30°). The NW-trending structures may not have experienced fresh water dissolution if closed at the time of formation. This may explain why their geometry is more subtle and cannot be traced by Passive ANT tracking.

The interpretation of the two sets of faults/joints would be more reliable if 3D seismic coverage extended northwest of the North Boundary. Because these features are a major concern for seal quality, the acquisition of new 3D seismic data in the entire area is strongly suggested.

Curvature volumes and confined features

Features revealed by maximum negative and positive curvature are shown by Fig. 1-8a-e. These features are less-linear than those revealed by ANT as shown in Fig. 1-4, although some features superimposed on the lineation revealed by ANT. The connectedness, or the continuation of these curvature features, both laterally on slices and vertically in profiles, is not as good as those shown by ANT volumes. From the slice-view, these features are most likely individual patches bound by the high values of maximum positive curvature, or patches with low maximum negative curvature values. The patch dimension ranges from 300 to 600 ft in diameter, and 20 -70 ft in depth. Displays with varying ranges of curvature scales (upper and lower limits) do not significantly change the relative dimension of these features. High curvatures at this scale are likely indicating karst topography and/or dissolution-related porous. However, such dissolutions are more pronounced along planes of weakness, such as fracture zones associated with faults.

The vertical time window for the curvature computation is 10 ms, much greater than the vertical depth window between slices. However, a faint trend of increasing patch size is shown going from shallow (Fig. 1-8a) deeper slices (Fig. 1-8d). As seen from a comparison between the two slices at -1500 ft TVDSS and -2050 TVDSS (Fig. 1-8e), curvatures seem to be less complicated at the deeper slice around Gilmore City (-2050 TVDSS) with larger patch sizes. With smaller patch sizes, they become more significant (or more complicated) upward to the shallower strata which is above Fort Scott Limestone (-1500 ft TVDSS).

If the pattern shown by curvature features reflect a system of faults and fractures due to regional structural deformations, it is likely to be more complicated in older

carbonate strata then in younger clastic and carbonate interbedded strata, in contrast to the trend of patterns shown in Fig 1-8e. This supports the conclusion that volumetric curvature for land 3d seismic data of this quality may be indicating features in the data largely unrelated to faults and fractures.

As stated in the March 31, 2009 report, curvature features revealed more confined than unconfined features. Confined features can have different origins, including differential dissolution or re-crystallization within different depositional facies by early or late diagenesis processes after burial, or dissolution on karst topography during exposure and erosion of the strata (e.g., Mississippian and Gilmore City unconformities). The lateral distribution of points or planes of weakness are primarily controlled by depositional facies in carbonate build-ups (Carr et. al., 1999) and secondarily by the orientation of faults, joints and fractures. The vertical penetration of karst is controlled by the amplitude of uplifting (or sea level fluctuation) while the maturity of the karst topography is a function of the duration and stability of the exposed strata. The major karst developments are thought to be on the Miss. unconformity, and secondary GMC unconformity. The karst dissolution might even occur on the less significant boundary of the upper Osage, which was thought to represent at least depositional hiatus and therefore was once exposed for a period of time (Carr, et. al., 1999).

Confined features formed on karst topography can be vertical, horizontal, or with other preferred orientations at a very low dip angle within stratigraphic bedding. Vertical sink holes represent the early stage of karst development during rapid drop of water table (due to uplifting or sea-level drop) with the penetration depth from surface down to the water table. During this stage, the surface drainage system may be partially or entirely destroyed by sink holes. Horizontal tunnels or collasped channels connecting sink holes represent the mature stage of karst development associated with a relatively stable water table and features concentrated near the water table. If viewed from a vertical stratigraphic section, all these features tend to occur/concentrate as confined layers with limited vertical penetration. A conceptual model of karst development in carbonates is shown in Fig. 1-8f (Marshak, 2001).

Slices from chaos and variance volumes, useful for visualizing confined features (as shown by Fig. 1-4, c and d), further validated the above observation and interpretation of confined features from curvature analysis.

When volume attributes chaos and variance are sliced at Ft. Scott depth (Fig. 1-9a-b), nearly featureless surfaces are revealed except for a few high values related to faults/joints also indicated by ANT volumes. Slices for both volumes at the Mississippian unconformity (Fig. 1-10a-b) show significant lateral variation. This represents the major period of regional deformation and erosion, thereby allowing longer development for karst topography. The chaos and variance are dominated by horizontal elongate patchy features (channels) and faults/joints revealed by ANT. Similar patterns below the Mississippian unconformity have weakening lateral continuity as seen from slices slices at the oil-water contact (Fig. 1-11a-b) and Gilmore City (Fig. 1-12a-b). Some nearly circular features in older strata about 100 ft below Gilmore City (Fig. 1-12c), are probably sinkholes formed at an early stage of karst development.

A similar trend can be seen from the local dip volume attribute. At the oil-water contact (Fig. 1-13a) many high dip features have lateral continuity, likely related to channels that have steep boundaries and relatively flat centers. A weak indication of high dips are observed following NE or NW faults. However, in a deeper slice near Gilmore City (Fig. 1-13b) the contrast between high and low dip values becomes less significant. Some curved high dip features surrounding isolated patches with very low dip values (Fig. 1-13b) cannot be seen clearly on the shallower slice. Similar to the high maximum positive curvatures around concave patches, these high dips around relative flat patches may be walls of karst sink holes. However it should always be borne in mind that volumetric dip is responding to seismic slopes in the time data (even when converted to depth), and there are many locally sloping events that are unrelated to geology (noise, processing artifacts, near surface problems, etc.).

The interpretation of features shown by the local azimuth volume attribute is less straight forward as other attributes, as seen from depth slices at the oil-water contact (Fig. 1-14a) and Gilmore City (Fig. 1-14b). Confusion can arise because there are two azimuth quantities involved, (1) the attribute itself with is the compass direction of the maximum dip computed locally in the seismic volume, and (2) the map-view orientation of features

in the attribute map. For example, at some location in the depth slice we might have an azimuth attribute value of 90° (orange), meaning the local seismic dip is pointing east, and this orange feature is linear oriented at azimuth 360°, meaning it is trending north-south. In our discussion we distinguish these two by the terms 'azimuth' (the attribute) and 'orientation' (the map-view alignment), both on a clockwise-from-north 0-360 notation.

Fig. 1-14a-b has the overall appearance of being almost random, but locally shows an interesting pattern. The red-black arrow highlights one of several azimuth 60° features (NE dip, red arrow) are oriented in the 330-340° direction (NW, black arrow), pattern also seen at the Gilmore City level (Fig. 1-14b). Somewhat more questionably, at the OWC (Fig. 1-14a) the blue-black arrow indicates an azimuth 310° (NW dip, blue arrow) feature oriented at 40-50° (NE, black arrow). This seems still present, but less developed, at the Gilmore City level (Fig. 14-b). In some locations at both levels, these two trends intersect with visible offset (black circles), although not in the same direction.

More observations on the Azimuth volume displayed at different depth and overlaid with slices from ANT and other volumes are needed to provide a satisfactory explanation for these features.

Reservoir Property Computation and Property Grids

Accomplishments made for the property modeling of shallow reservoirs include correction of 17 neutron porosity logs based on lithology, correlation corrected porosity logs with core porosity measurements from 2 wells, and permeability estimation based on the regression of core porosity and permeability data. Property modeling of deep saline aquifer is based on logs from two wells (no core measurements available) and a poro-perm 26-field study of the Mississippian Osage 'Chat' (Alan, Guy, and Watney, 2002). ['Chat' is an informal name for Mississippian-age Osage cherty dolomite] Results include permeability estimation and propagation with the aid of depth-converted seismic impedance volume re-sampled at zone surfaces.

Porosity

To calculate porosity from neutron log data it is necessary to assume a lithology, with raw log values typically recorded in limestone porosity units. For lithologies other than

limestone, it is necessary to convert apparent limestone porosity units to corrected porosity units. This is important for reservoir characterization since limeston porosity values may be up to 5% higher than real values in dolomite, and up to 8% lower than real values in sandstone. Figure 2-1 shows relationships derived for correction of apparent limestone neutron porosity to other lithologies.

Our data set includes two wells with both neutron logs and core porosity. This allows us to develop a relationship between core porosity and neutron porosity in these two wells (Fig. 2-2, and also Fig. 17b of March 31, 2009 report). The derived relationship is very poor (-0.2 correlation coefficient), but is the only data available in the field. From this equation, pseudo-core porosity was derived from 18 litho-corrected neutron logs for the two shallow reservoirs (lower Cherokee and Warsaw). This in turn was used to compute permeability based on the relationship between core porosity and core permeability.

As an initial step, the above procedure was applied to the zone-averaged porosity values only, implying no vertical variations in porosity for all grid cells within each litho-zone. Fig. 2-3a shows the zone-averaged uncorrected neutron porosity for the Fort Scott. Within the 3D seismic survey boundary the lowest value is less than 9%, after correction Ft. Scott porosity is no greater than 8%. There is no core measurement available to validate this result. Fig. 2-3b shows the zone-averaged uncorrected neutron porosity for the Lower Cherokee sandstone reservoir. The only core porosity measurement for this formation is 11% in the Dickman 4 well. Fig. 2-3c shows the zone-averaged porosity for the Miss. Salem and Warsaw limestone interval containing the carbonate reservoirs. Corrected porosity values (not shown) have the same general appearance as the uncorrected values, with absolute porosity differences of +/- 6%.

The corrected shallow reservoir porosity maps are one input for the CMG flow simulator. The maps are not yet available for the deep saline aquifer. The data set for the simulation input is estimated from analogs as will be described at the end of this section.

Permeability

Core permeability measured parallel and perpendicular to bedding across all formations has a correlation coefficient of 0.9 (Fig. 2-2). Therefore only horizontal permeability is estimated and the relationship in Fig. 2-2 is used to calculate vertical permeability.

Together with the 5 wells with core porosity only, there are 22 total control points for computing the permeability for the shallow reservoirs. Estimating permeability from porosity is based on the relationship shown in Fig. 17a of March 31, 2009 report, resulting in a Ft. Scott permeability map (Fig. 2-4a). There are no core measurements to validate this map, but in general the computed permeability seems relatively high. For the lower Cherokee sandstone (Fig. 2-4b), we have one core measurement of 42 md, within the range of computed values. For the Mississippian-Osage interval, the resultant permeability values are generally lower than core measurements. The maximum permeability is 200-800 md (the latter might be due to fracture) as seen in the Dickman 4 and 5 wells. Accuracy is limited by data availablity to generate the relationships between permeability and porosity.

Shallow reservoir permeability may not be homogeneous. As indicated by core measurements (Fig. 2-2a), max horizontal perm is greater than maximum vertical perm by least 20%. This suggests that the reservoir conductivity may not be controlled by vertical fractures, but confined dissolution features as revealed by seismic attributes (curvature, variance, and chaos).

Properties for the deep saline aquifer

Core porosity from nearby Schaben Field (Fig, 17c of the March 31, 2009 report) is used to correct neutron, sonic, and density porosity for the two wells that penetrate the deep saline aquifer at Dickman (Humphrey 4-11, and Sidebottom 6). They exhibit a similar range of corrected porosities. An initial approximation of permeability from porosity was derived as : $k = 0.0018e^{0.4313*\phi}$, excluding core intervals with vuggy porosity. Porosity and permeability data from a study of Osage Chat in 26 Kansas oil fields (Alan et. al., 2002) was also used for quality control purposes. In this data set, the core porosity is relatively high due to vuggy zones, up to 45% (Fig. 2-5), and the relationship between perm an whole core porosity is: $\log(k) = 0.067*\phi - 0.53$. These two relationships were used to estimate the permeability of the deep saline aquifer at two wells with corrected porosity data and uncorrected neutron porosity logs (Fig. 2-6).

In order to fill the gap between the two deep saline aquifer control wells, the depth-converted seismic impedance volume can be used to aid property propagation. The impedance volume used from inverted from the all offset migrated stack. As shown

by the Fig. 18 of the March 31, 2009 report, a high correlation coefficient ranging from 0.7 to 0.73 was obtained between the impedance and porosity logs in the two control wells. The geological model we have developed for Dickman extends from Ft. Scott down to the Gilmore City. Depth-converted impedance volume slices at the Fort Scott (Fig. 2-7) and Gilmore City (Fig. 2-8) reveal similarity and consistency that suggests impedance can useful as a guide to propagate porosity and permeability throughout the model, but particularly so in the deep saline aquifer with only two well penetrations. However, the major challenge is to resample the impedance values at all grid cells and to standardize the re-sampled values. This task will be completed during the next reporting period.

Reservoir Simulation

Flow Simulation Work

We divided the flow simulation work into three parts: pre-simulation work, Dickman field history matching and the simulation for deep saline aquifers. Pre-simulation work includes literature review, selection of simulators and Dickman filed appraisal, and has been completed in the previous quarter and will be not discussed in this report. Dickman history matching simulation is the major task of the current quarter. The simulation for deep saline aquifers will be the major task for the rest of the year.

Dickman Field History Matching

The shallow geologic section forms the cap rock for the deep saline aquifer system which is our CO_2 sequestration target. A good understanding of the shallow section is essential for safe CO_2 storage in deep saline aquifers. Dickman field history matching will provide us a good opportunity to understand the shallow reservoir.

The conventional roles of history matching are to test and improve a reservoir model. The reservoir property data, formation structural data and production data collected from geological model analysis and the production company will be validated or calibrated through the history matching process. Some suggestions will be made to the geoscience team to improve the existing reservoir model.

According to the model analysis, Dickman field consists of two geological reservoirs: Lower Cherokee sandstone and Mississippian carbonate. The Mississippian can be further divided into a low-porosity interval above a high-porosity layer. Figure 3-1 shows the locations of all 22 production wells and the top map of Dickman field.

A known fault cuts through the upper left corner of the reservoir. All production wells are located on the southeast side of the fault and several production wells are very close to it. This is strong evidence that the fault represents a flow barrier. Geological analysis indicates it is a normal fault and most likely became sealed due to post faulting diagenetic alterations. For simplicity, we treat N-E fault as a sealed fault.

Four production wells (Schaben 1,2 4 and 5-19) are located on an area close to the south boundary of the map. The Lower Cherokee top in this area is below the oil water contact level (OWC). Further investigation indicates that these four wells have a production zone at least 40 ft higher than the Lower Cherokee formation top surface. We will exclude the four wells from the history matching simulation at this time and redo the history matching simulation after the pay zone data for these four wells are available.

The elevation of the south-east corner of the Lower Cherokee map (Fig. 3-1) is higher than OWC but without production. For simplicity, we will assume a low permeability value for SW corner area in the simulation model.

A depth structure map on the Mississippian porous carbonate zone is shown in Figure 3-2. At location A the pay zone is from a stratigraphically higher formation above the simulation target. At location B the target carbonate reservoir is partially missing. The Lower Cherokee Sandstone and the remaining Miss. carbonate have relatively low permeability.

Figure 3-3 shows edited Lower Cherokee formation top map and production wells after removing the north-east part of the original map and four production wells as discussed above.

A Dickman field pre-simulation data appraisal was completed in the previous quarter. According to Merriam (1963), the Dickman field was discovered and put into production in 1962. From Grand Mess Production Corporation, we obtained the

production data for 22 wells. The cumulative oil production at the end of 2008 is about 2.3 million bbl and the cumulative water is about 12.2 million bbl. There is no gas production. The other known reservoir properties are:

1. the reservoir acreage = 240
2. Net thickness = 7 feet
3. Oil API gravity = 37
4. Reservoir Temperature = 121 F
5. Average Depth = 4424 feet
6. Pressure at 4424 feet depth = 2200 psi
7. From the production data, the estimated reservoir porosity is about 0.2

The following data were provided by the geological and geophysical model analysis:

1. The formation top and thickness maps for Low Cherokee pay zone
2. The formation top and thickness maps for Mississippian pay zone
3. Reservoir porosity map

In addition, the model analysis indicated that the Mississippian reservoir can be further divided into two layers, a low porosity and low permeability layer on the top of a normal porosity and normal permeability layer. Unfortunately, the following data are not available at this time

1. Permeability data
2. Production well pressure
3. Well perforation data
4. Reservoir fluid Pressure, Volume, Temperature (PVT) date

We have to make assumptions on the permeability data and find PVT data using analytic correlation curves.

Figure 3-4 is the initial simulation grid constructed for the history matching simulation. The grid size is 55 x 55 x 10 and the size of each grid is 250 x 250 ft, and a total simulation grid layers. The first four layers are for Lower Cherokee, the next two

layers for the low porosity Mississippian layer and the last four layers for the high porosity Mississippian layer. Table 2 shows the assumed permeability for each simulation layer. For the southeast corner of the grid, we assume permeability and porosity as 2 md and 0.02, respectively. The numerical experiment took about 30 minutes to complete a single history matching run on a laptop computer.

Figure 3-5 is another simulation grid used for history matching. In this model, we exclude the low permeability and low porosity area (the southeast corner area as shown in Figure 3-4) from the simulation grid and adjust orientation so that one axis is parallel to NE fault. The grid size reduces to 73 x 33 x 10, and computation time drops to10 minutes for a single history matching run. Several different oil water contact (OWC) levels have been proposed by the log analysis. After trial history matching runs, we chose OWC of -1957 TVDSS for the simulation model initial condition.

Table 3 is the cumulative oil and water production comparison between real production data and simulation data. There is significant difference between two sets of numbers for this initial simulation model, likely due to a variety of factors related to the model being too simple. The fluid PVT data and relative permeability data also need to be adjusted in order to match the oil water ratio.

Figure 3-6 shows Dickman field pressure distribution at the end of simulation. Because the well pressure data are not available, we cannot compare the computed pressure with the real pressure at this time. The pressure distribution is directly related to the permeability. The pressure matching is normally used to validate or calibrate the reservoir permeability property.

Table 4 lists the reservoir top depth at each production well location. The depths at several well locations including Elmore 1, Stiawalt 2, Tilley 1b, and Tilley 5 are lower than the OWC (-1957 TVDSS) used in the simulation model. This problem may be due to incorrect formation tops, production belonging to an unknown pay zone, or Lower Cherokee and Missippian being two independent reservoir units with different OWCs.

Because of the lack of permeability data, we have not yet achieved a satisfactory matching result on the water oil ratio and water break time for each individual well. We will continue history matching work on the next quarter.

The simulation for deep saline aquifers

Deep saline aquifer represent the most important venue for CO_2 storage because it has the largest storage capacity among all formations present, included coal seams and depleted gas reservoirs. Storing CO_2 in deep saline aquifers also avoids the possibility of CO_2 escape through corroded well pipes, a major concern about CO_2 storage in depleted petroleum reservoirs. Computer Modeling Group's GEM simulator will be used in this research. The GEM simulator will enable us to find an optimal CO_2 injection process and to monitor underground CO_2 movement for a long periods. Performing simulation on the deep saline aquifer will be the major task for the rest of the year. Some pre-simulation data assessment has been completed in the current quarter.

Evaluation on the targeted CO_2 storage site

After assuming certain reservoir properties, we are able to estimate the aquifer area requirement for the storage of a given amount of CO_2 before performing simulation. Using the MIDCARB CO_2 sequestration calculators (www.midcarb.org/calculators.shtml) with reservoir temperature of 121 F and pressure 2200 psi, we find that CO_2 is in the super-critical state with density about 0.7 ton/m^3 and volume brine solubility of about 64 ton per acre-ft.

As shown in Figure 3-7 (Metz et al, 2005), after injection CO_2 will be initially trapped in three forms; a free or super-critical gas (structural trapping), an immobile gas in the porous media (residual gas trapping), or a dissolved gas in brine (solubility trapping). Assuming aquifer porosity of 0.2, and irreducible water saturation of 20%, one acre-foot aquifer is capable of trapping

1233 (m^3 per acre-foot) * 0.2 * (1-0.2)*0.7 ton/m^3 = 140 tons

of free or super-critical CO_2. Assuming aquifer rock residual gas saturation as 10%, one acre-foot of aquifer rock on average can trap

1233 (m^3 per acre-foot) * 0.2 *0.1*0.7 ton/m^3 = 17 tons

CO_2 as immobile residual gas. On the other hand, the same volume of aquifer rock can dissolve

64 (ton/acre-ft) *0.2 = 13 ton of CO_2.

Free or super-critical CO_2 can escape to the atmosphere through a faulted or fractured cap rock. In a depleted hydrocarbon reservoir, free CO_2 also can escape to the surface through corroded well pipes. Only residual gas trapping and solubility trapping are considered to be safe long-term CO_2 storage processes. As time passes, CO_2 will be first dissolved into brine then be mineralized. So we are going to use CO_2 solubility in brine as a criterion to determine the minimum aquifer volume required for a long-period simulation prediction. For example, in order to dissolve 1 billion tons CO_2, we need

1,000,000,000 tons / (13 tons/acre-ft) = 77 million acre-ft aquifer rock volume

If the average aquifer thickness is about 1000 ft and the net to gross ratio is 0.1, such volume of aquifer rock will cover an area of 770 thousand acres, which is about 1,000 square miles.

The western interior plains and Ozark Plateau aquifers (Fig. 3-8), form the saline aquifer system under the state of Kansas and cover several hundred thousand square miles. The aquifer system is stable with water flow velocity of only about 40 feet per million years, which excludes the possibility that the injected CO_2 will be migrated to the surface through the aquifer water flow. The aquifer system proposed in this research is an ideal carbon dioxide storage target.

Work Plan for the Next Quarter

Geology

Four remaining issues so far in this study are the major focuses for the next reporting period.

1. The re-adjustment of results in geometry and property of the shallower reservoirs based on the first round results of "history matching" by the CMG simulator. This will take several iterations until an optimized history matching result that can be used for predictive modeling is obtained.
2. The propagation of porosity and permeability into the grid for the Upper Osage deep saline aquifer, with the aid of seismic impedance volume. This will produce an input data set to CMG simulator for the flow simulation of deep saline aquifer.

3. A literature research on the structure framework and deformation history of the strata in Kansas, focusing on the Ness County area, in order to better understand the type, mode, property and motivation history of the faults/joints and fractures interpreted from seismic geometry studies. Volumetric attributes may be integrated together for a better visualization. This will provide not only constraints to the flow simulation but also necessary information on the quality of seals for the CO_2 sequestration.
4. Run the ECLIPSE "Black Oil Simulator" on Petrel using the improved M3 structural and property grid. The results will be compared with results generated by CMG flow simulator.

Geophysics

Further work will be done to improve synthetic seismogram quality and related time/depth curves.

Reservoir Simulation

As mentioned before, performing simulation in deep saline aquifers is the major task of the next quarter. The final object of this study is to build a full field model and to provide a prediction for long period of CO_2 safe storage. We understand that the effectiveness of the simulation model depends on the completeness and accuracy of the data collected. The first priority work of the next quarter will be to build a simple one injector model to validate and calibrate the data obtained from the geological and geophysical model analysis and other sources.

Cost and Milestone Status

Baseline Costs Compared to Actual Incurred Costs

2009			
Apr 1 – Jun 30	**Plan**	**Costs**	**Difference** Plan minus Costs
Federal	$25,000	$26,744	($1,744)
Non-Federal	$9,410	$0	$9,410
Total	$34,910	$26,744	$7,666

Forecasted cash needs vs. actual incurred costs

Notes:

1. Federal plan amount based on original award of $400K averaged over 12 reporting quarters.
2. Cost this period reflects 3 months salary for J. Zeng and P. Geng, and 2 months for H. King
3. Non-Federal plan amount based on original budget cost share of $150,573 averaged as above.

Actual Progress Compared to Milestones

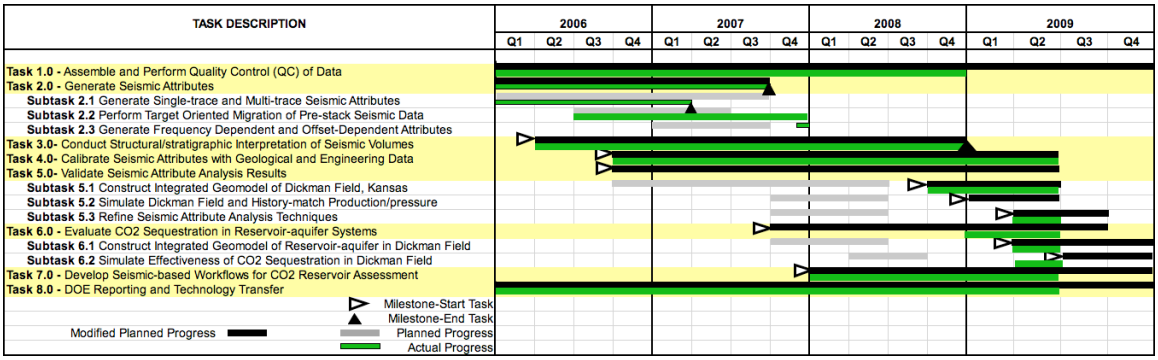

Summary of Significant Events

Problems and Significant Events

No problems to report. During this period a new proposal was submitted to DOE involving a reshoot of the Dickman 3D seismic survey using simultaneous sources, multicomponent receivers, tighter data spacing, and higher density data. All of this would generate a seismic data set tuned for the challenges of CO_2 sequestration – subtle fault and fracture mapping, better rock property estimation, and higher resolution to detect geological features of interest.

Continuing Personnel

Prof. Christopher Liner is Principle Investigator and lead geophysicist. He is a member of the SEG CO_2 Committee, Associate Director of the Allied Geophysical Lab, and has been selected to deliver the 2012 SEG Distinguished Instructor Short Course.

Dr. Jianjun (June) Zeng has been working exclusively on this project since Dec 2007 and is lead geologist. She will be funded through the end of 2009.

Heather King is a graduate MS student in geophysics who joined the project in January 2009 as a research assistant. She will be funded out of the project Jan-May and Sept-Dec 2009, when she anticipates graduating. Her thesis will focus on Fort Scott to demonstrate the integrity of this formation as a seal for injected CO2. This will involve subtle structure and stratigraphy inferred by interpretation of multiple seismic attributes.

Dr. Po Geng has been working on this project as a specialist consultant since February, 2009. He will be funded out of the project, considered part-time, through the end of 2009.

Technology Transfer Activities

An abstract on the Dickman CO2 sequestration simulation was submitted to the SEG, 2009.

Contributors

Christopher Liner (P.I, Geophysics)
Jianjun (June) Zeng (Geology and Petrel Modeling)
Po Geng (Flow Simulation)
Heather King (Geology and Geophysics, MS Candidate)

References

Abers, G. , C. Z. A.Mutter, and J. Fang ,1997, Shallow dips of normal faults during rapid extension: Earthquakes in the Woodlark-D'Entrecasteaux rift system, Papua New Guinea: Journal of geophysical research, 102, 15301-15317

Merriam D., 1963, Geologic History of Kansas, KGS database, Kansas Geological Survey Bulletin 162, http://www.kgs.ku.edu/Publications/Bulletins/162/08_patt.html

Alan P. B., W. J. Guy, and W. L. Watney, 2002, Characterization of the Mississisippian Osage Chat in South-Central Kansas: Kansas Geological Survey, Petroleum Technology Transfer Council workshop presentations, http://www.pttc.org/workshop_presentations.htm

Carr, T. R., D. W. Green, and G. P. Willhite, 1999, Improved oil recovery in Mississippian carbonate reservoirs of Kansas: Near term-class 2, Annual Report Submitted to US Department of Energy (DOE), Report no. DOE/BC/14987-10, 168.

Franseen, E. K., T. R. Carr, W. J. Guy, and D. S Beaty, 1998, Significance of depositional and early diagenetic controls on architecture of a Karstic-Overprinted Mississippian (Osagian) reservoir, Schaben Field, Ness County, Kansas: Presented at the AAPG Annual Meeting.

Franseen E. K., 2006, Mississippian (Osagean) Shallow-water, mid-latitude siliceous sponge spicule and heterozoan carbonate facies: An example from Kansas with implications for regional controls and distribution of potential reservoir facies: Kansas Geological Survey, Current Research in Earth Sciences, 252, part 1.

Marshak, S., 2001, Earth: Portrait of a Planet, W. W. Norton, N.Y.

Nissen, S. E.,T. R. Carr, and K. J. Marfurt, 2006, Using New 3-D Seismic attributes to identify subtle fracture trends in Mid-Continent Mississippian carbonate reservoirs: Dickman Field, Kansas, Search and Discovery, Article #40189.

Marfurt, K., 2009, 3D Seismic Attributes, AAPG Short Course.

Merriam, D. F., 1963, The Geologic History of Kansas: Kansas Geological Survey Bulletin, 162.

Metz, B., Davidson, O., de Coninck, H., Loos, M., and Meyer, L. A. (Eds.), 2005, IPCC Special Report on Carbon Dioxide Capture and Storage, Cambridge University Press, New York, N.Y.

OuYang. J., 1994, Well Log Interpretations and Reservoir Descriptions: Book Series on Petroleum Exploration in the Tarim Basin, 9, 235–291.

Timothy R. Carr, Daniel F. Merriam, and Jeremy D. Bartley, 2005, Use of relational databases to evaluate regional petroleum accumulation, groundwater flow, and CO2 sequestration in Kansas, AAPG Bulletin, v. 89, no. 12, pp. 1607–1627.

Tables

	Dip azimuth	Dip	Surface area	Azimuth in seismic	Dip in seismic	Mean input	Patch confidence
	90.50	89.91	6583.00	180.04	89.98	3.26	140.30
34	325.96	84.31	1383.00	55.46	89.23	2.30	22.79
	90.14	83.53	1520.00	179.60	89.11	2.68	27.94
48	15.27	81.87	2618.00	104.45	89.62	2.25	42.52
90	345.83	80.06	1593.00	75.54	88.96	2.23	25.75
45	72.72	79.72	2560.00	160.89	88.42	2.27	41.80
42	163.68	54.49	2116.00	251.78	87.25	2.27	34.57
40	224.37	37.05	2652.00	316.69	79.23	2.25	43.15
66	324.17	24.76	1214.00	57.83	77.80	2.23	19.60
68	142.95	22.30	1762.00	217.01	89.86	2.27	28.83
10	179.97	20.96	4232.00	267.79	71.13	2.36	71.05
17	221.82	20.53	1826.00	328.47	82.81	2.52	32.11
23	116.30	15.04	1009.00	9.62	00.50	2.20	29.64
84	160.85	15.11	1155.00	250.09	68.48	2.21	18.55
2	256.70	12.59	5723.00	346.53	56.74	3.03	115.29
19	128.76	8.67	2851.00	284.59	89.72	2.46	49.26

	Dip azimuth	Dip	Surface area	Azimuth in seismic	Dip in seismic	Mean input	Patch confidence
	270.41	89.72	1858.00	359.94	89.96	2.93	36.55
	181.99	87.76	1813.00	271.55	89.69	2.90	35.36
76	319.94	83.00	2322.00	48.99	89.29	2.43	39.80
2	49.29	58.92	3985.00	138.95	89.15	2.48	69.42
	272.43	46.93	2275.00	1.49	83.51	2.36	38.26
99	225.97	43.07	2261.00	315.52	82.63	2.31	37.42
14	46.87	34.68	5936.00	135.71	84.30	2.55	105.43
50	134.11	34.33	1310.00	219.28	82.62	2.36	22.01
44	146.56	30.97	2926.00	228.92	80.30	2.43	50.20
19	235.95	28.94	7245.00	328.08	74.05	2.61	130.91
56	348.56	28.85	2063.00	269.42	89.47	2.37	34.76
48	336.86	27.32	3511.00	67.34	79.22	2.53	62.01
29	209.12	25.03	4373.00	19.64	70.00	2.45	75.52
20	340.57	21.96	10403.00	69.02	69.31	2.52	183.29
	270.85	21.33	1270.00	356.21	73.18	2.57	22.68
41	42.79	19.25	2026.00	141.44	79.44	2.72	37.67
23	285.99	18.81	2709.00	15.33	70.95	2.51	47.53
22	149.46	18.63	7710.00	44.08	77.27	2.57	137.44
72	145.49	18.02	1634.00	51.53	64.86	2.43	28.06
71	62.62	17.66	2466.00	340.26	73.93	2.49	43.02
35	86.79	11.87	1513.00	176.41	55.87	2.42	25.85
34	160.32	7.21	1514.00	229.37	45.66	2.37	25.50
74	103.26	6.31	2541.00	98.48	45.74	2.35	42.57

Table 1. Parameters for some planes extracted from ANT volumes. Left: from Passive ANT volume, right: from Aggressive ANT volume. The planes with red dots are edge effects due to survey data boundaries (azimuths 360, 90, 180 and 270).

Simulation Layer	Permeability (md)	Porosity
layer 1	50	From Map
layer 2	250	From Map
layer 3	250	From Map
layer 4	50	From Map
layer 5	2	0.02
layer 6	2	0.02
layer 7	50	From Map
layer 8	250	From Map
layer 9	250	From Map
layer 10	50	From Map

Table 2: Permeability and Porosity data for Each Simulation Layer

	Production Data	Simulation Data
Cumulated Oil	1.75 million bbl	2.69million bbl
Cumulated Water	8.7 million bbl	69.5 million bbl

Table 3: Comparison between production and simulation data.

Production Well Name	Formation Top Depth(ft)
Dickman A1	1956
Dickman 1	1937
Dickman 2	1926
Dickman 3a	1932
Dickman 6	1957
Elmore 1	1959
Humphery 1	1948
Humphery 2	1950
Humphery 3-18	1951
Humphery 4-18	1949
Phelps 1a	1941
Sargent 5	1938
Stiawalt 1	1948
Stiawalt 2	1958
Stiawalt 3	1954
Tilley 1b	1957
Tilley 2	1946
Tilley 5	1967

Table 4: Dickman Field depth to top of simulator grid at each well location (TVDSS).

Figures

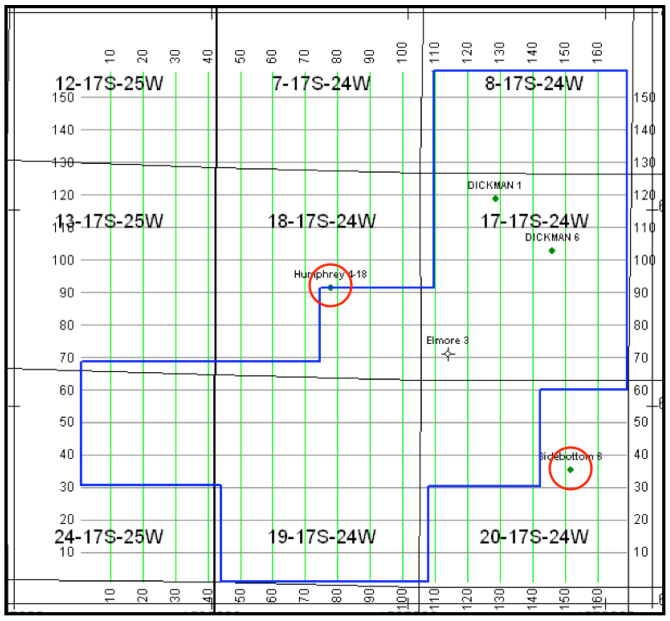

Figure 1-1. Wells with sonic (DT) logs used to compute interval velocity for depth conversion. Red circles indicate two deep wells that were projected to the nearest seismic trace in the 3D seismic image area (blue outline) so their DT logs can be used for interval velocity computation.

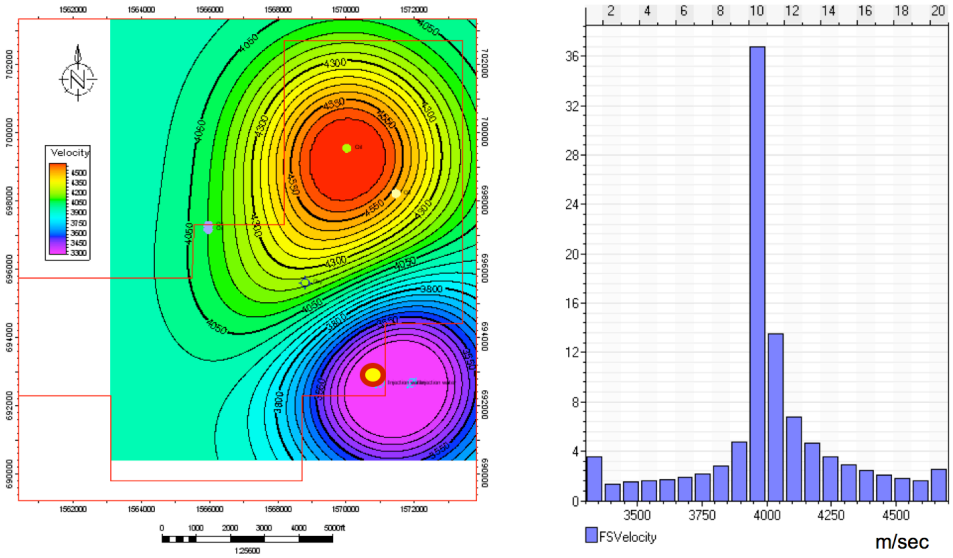

Figure 1-2a. Interval velocity distribution for Fort Scott interval. Interval velocity is peaked at 4000m/sec, and over 50% values are around 3940-4060 m/sec. Note the extreme low value at SideBottom 6 (red circle). This may caused by reasons other than lateral variations of rock acoustic properties and may be

related to different environment conditions of logging. As an input set for building a velocity model, the upper and lower 5-7% of velocity extremes in this distribution are eliminated.

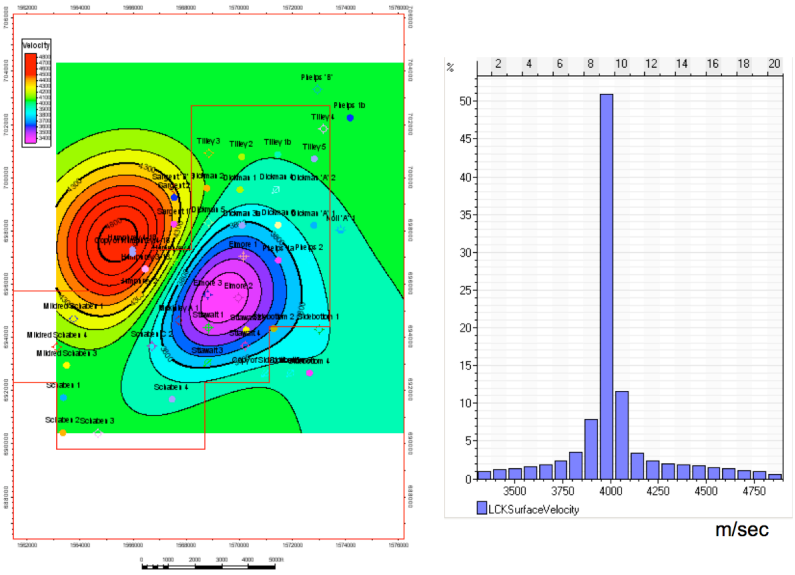

Figure 1-2b. Interval velocity distribution for Lower Cherokee (LCK) Sandstone. There are only three control wells because the LCK is missing in two wells. Values are widely scattered, but peaked at 4000 m/sec with over 50% values. Note the extreme low in Sidebottom 6 compared with other wells. As an input set for building a velocity model, upper and lower 5-7% of the velocity extremes in the distribution are eliminated. The range used is from 3700-4250 m/sec.

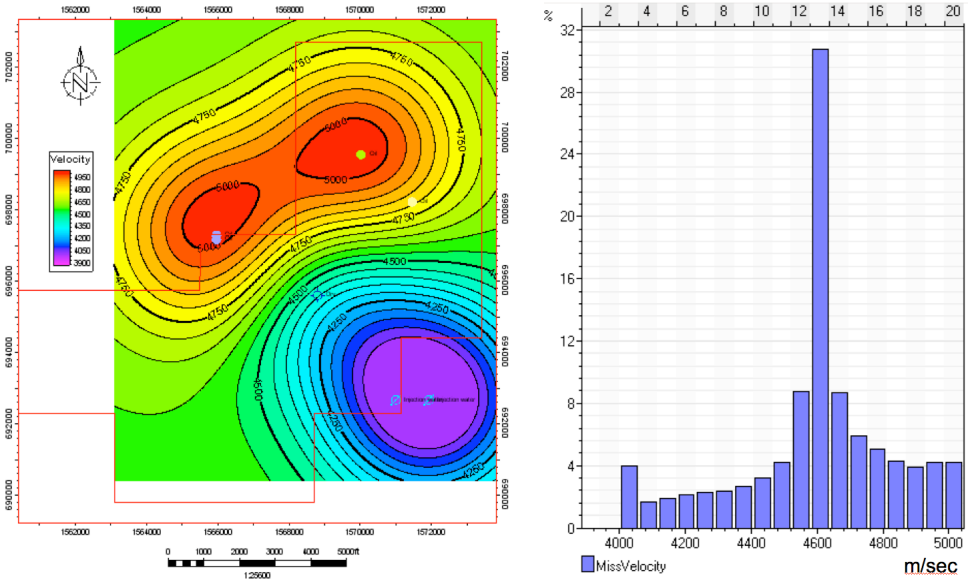

Figure 1-2c. Interval velocity distribution for Mississippian to Osage. Values are widely scattered, but peaked at 4600 m/sec. Over 50% are around 4550-4650 m/sec. Note the extreme low in Sidebottom 6 compared with other wells. As an input set for building a velocity model, upper and lower 5-7% of the velocity extremes in the distribution are eliminated. The range used is from 4150-4950 m/sec.

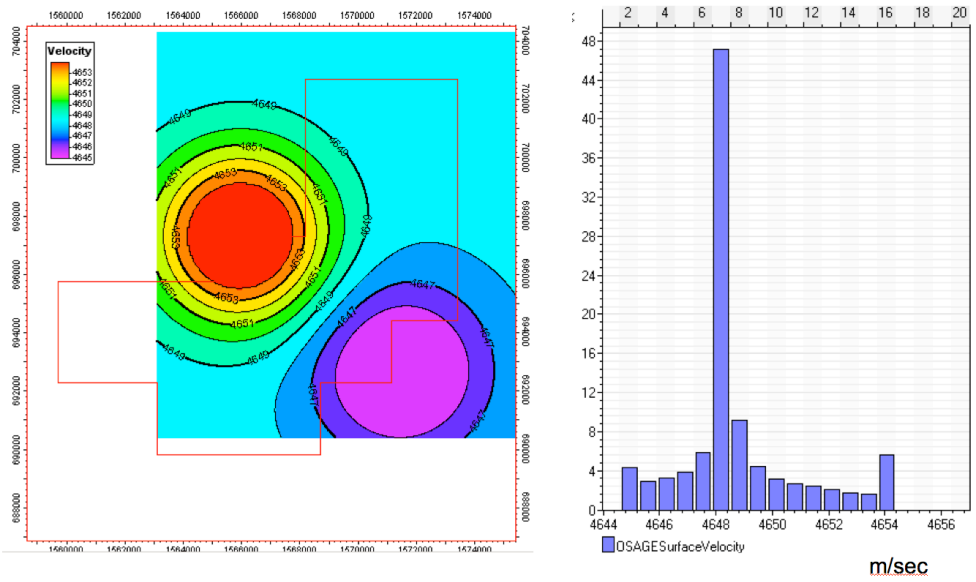

Figure 1-2d. Interval velocity distribution for Osage to Gilmore City (GMC). With only 2 control points, values range from 4646-4654m/sec, and 50% at 4648 m/sec. Note the extreme low in Sidebottom 6. As an input set for building a velocity model, upper and lower 5-7% of the velocity extremes in the distribution are eliminated. The range used is from 4646-4654 m/sec.

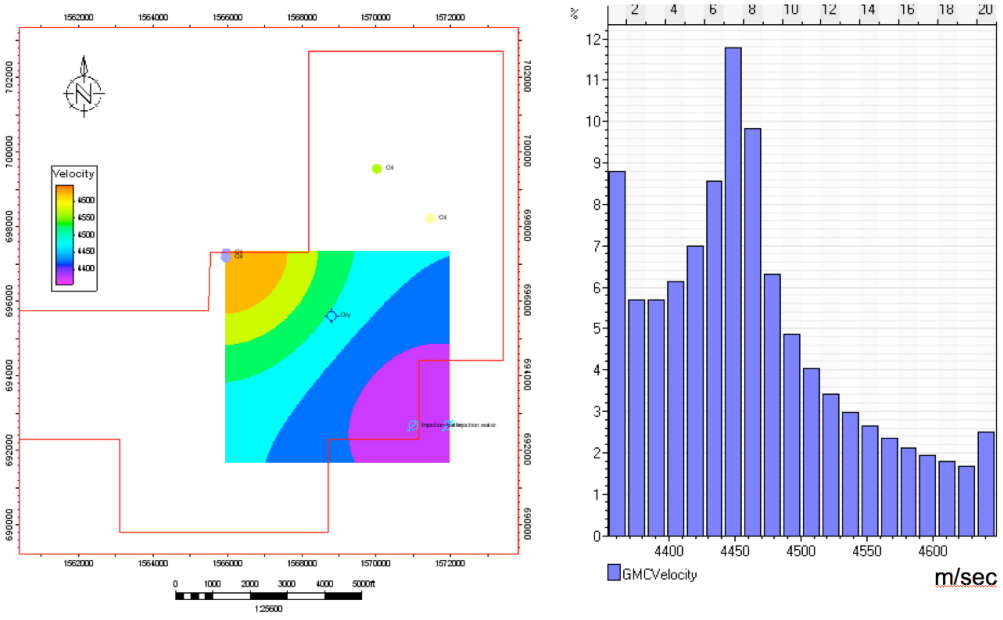

Figure 1-2e Interval velocity distribution for GMC and below. Being the deepest interval, this zone is poorly controlled by only two control points. Velocity values range from 4360-4660m/sec.

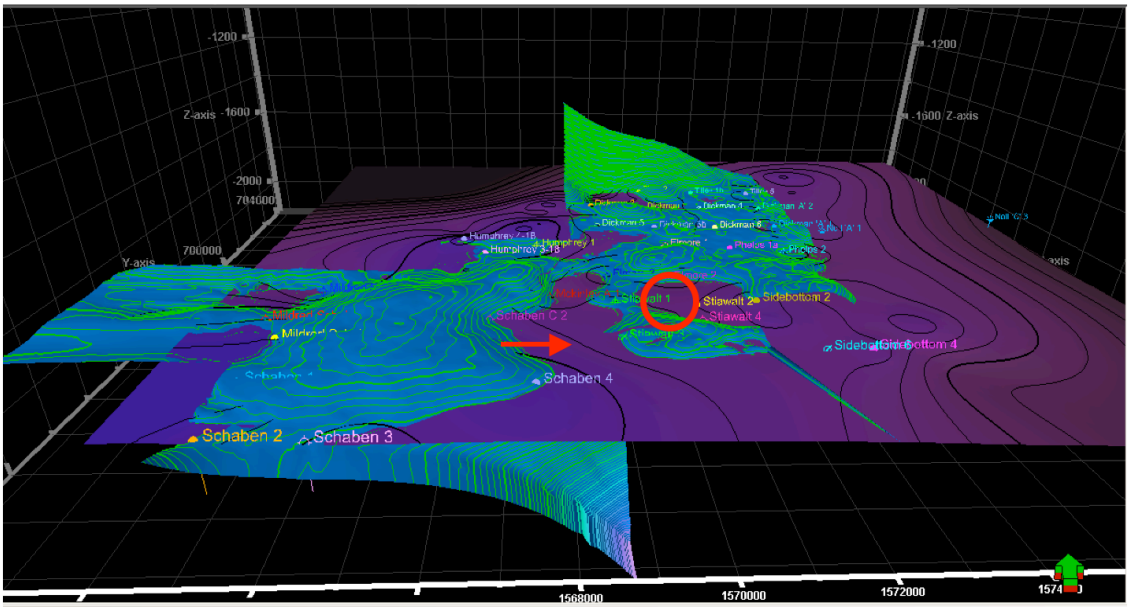

Figure 1-3a. Fort Scott well depth vs. depth-converted seismic horizon (vertical exaggeration 5:1). The well top surface is shown by black contour lines on purple background, and the depth-converted seismic surface is shown by light green contours on blue background. There are 35 data points (wells) for the conversion, and error is less than 2 ft at most controlling wells such as the Staiwalt 5-20 (red circle). Significant errors are in areas toward the north and south margins of the survey area that lack control points. In the central channel bend area (red arrow), the seismic surface is slightly below the well top values.

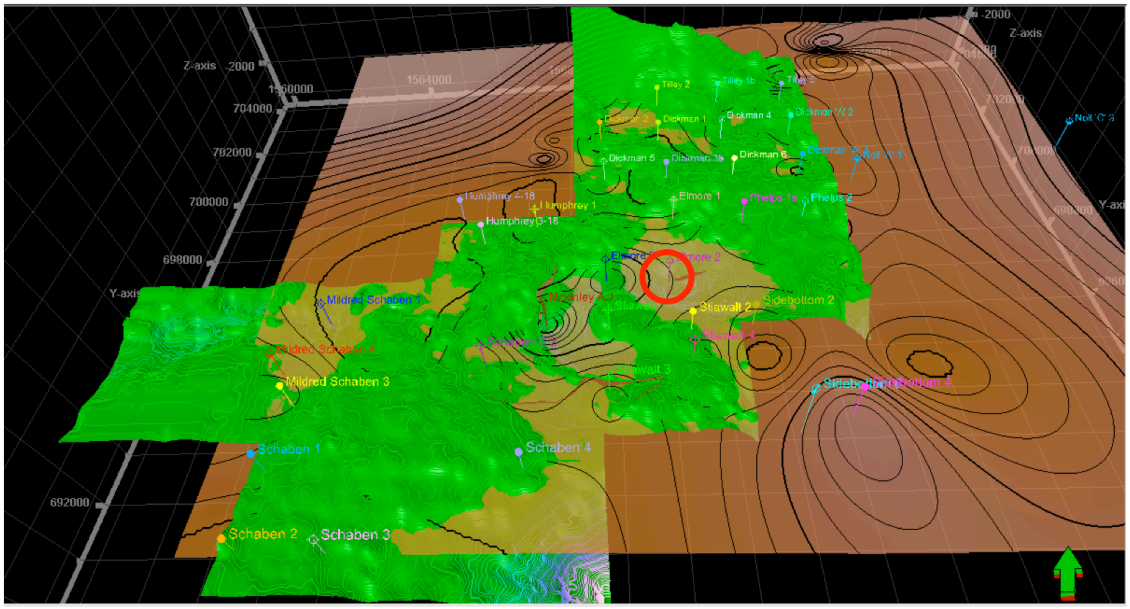

Figure 1-3b. Top Mississipian well depth vs. depth-converted seismic horizon (vertical exaggeration 5:1). There are 17 data points (wells) contributing to the depth conversion and less than a 6 ft error at most controlling wells. For example, error at the Elmore 2 is 6 ft (red circle). Significant errors are in areas toward the north margin of the survey beyond control points.

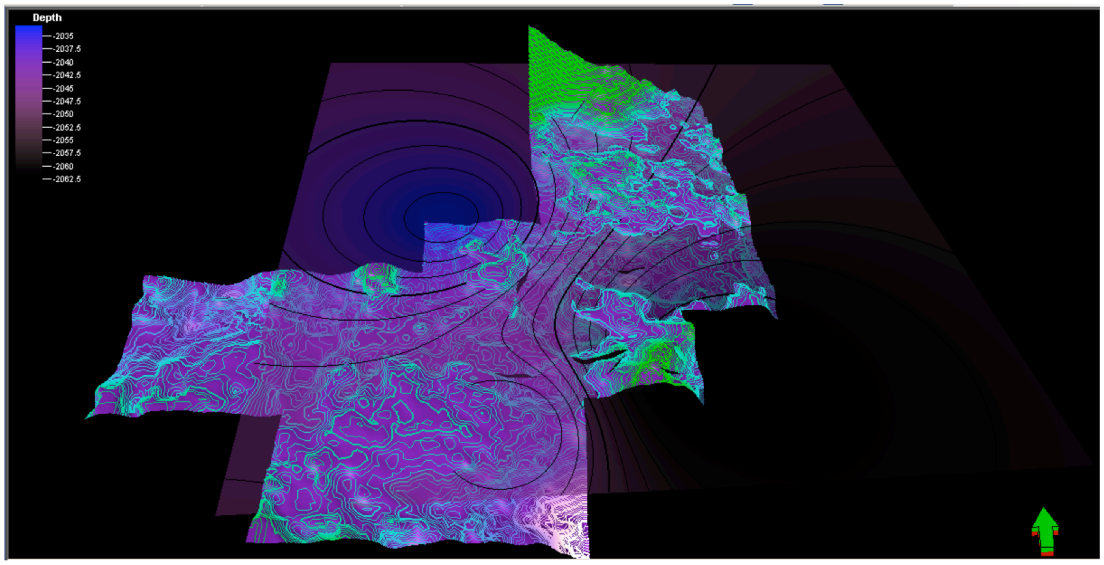

Figure 1-3c. Upper Osage dolomite well depth vs. depth-converted seismic horizon (vertical exaggeration 5:1). The surface from raw well tops data is shown by black contour lines and the surface of depth-converted seismic horizon is show by light blue contour limes on pink background. There are only 4 wells contributing to the well top surface, while the seismic interpretation details topographic features between wells. The scale bar on the upper left has a range of 2.5 ft. Maximum error is 6 ft between the two surfaces.

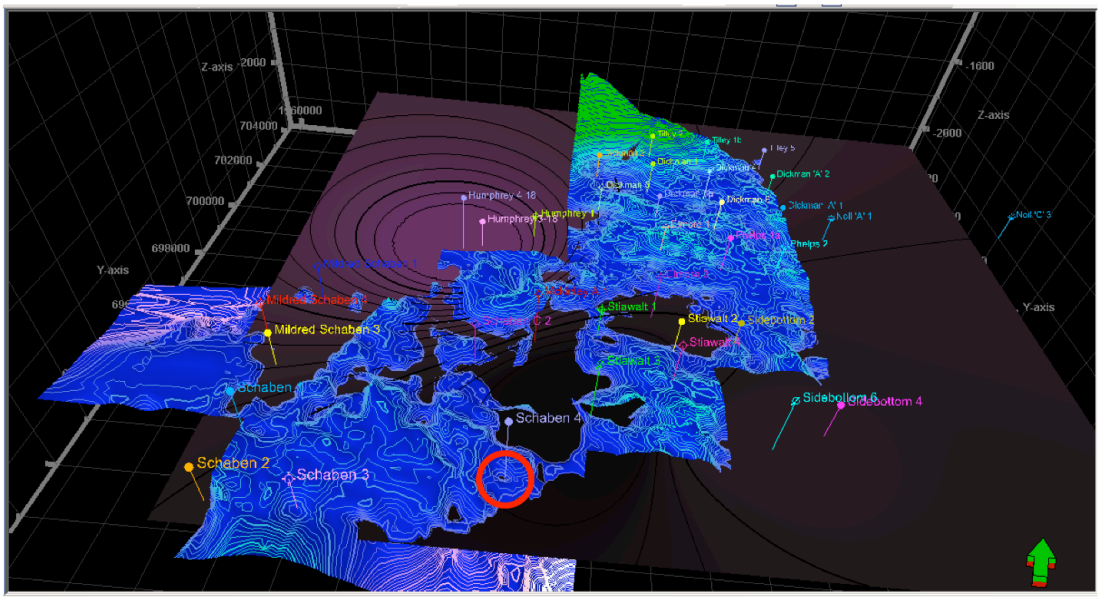

Figure 1-3d. Gilmore City well depth vs. depth-converted seismic horizon (vertical exaggeration 5:1). The well-top surface (3 wells contributing) is shown by black contour lines on purple background and the depth-converted seismic horizon is show by light blue contour lines on blue background. Error is at Schaben 4 well (red circle) is 12ft.

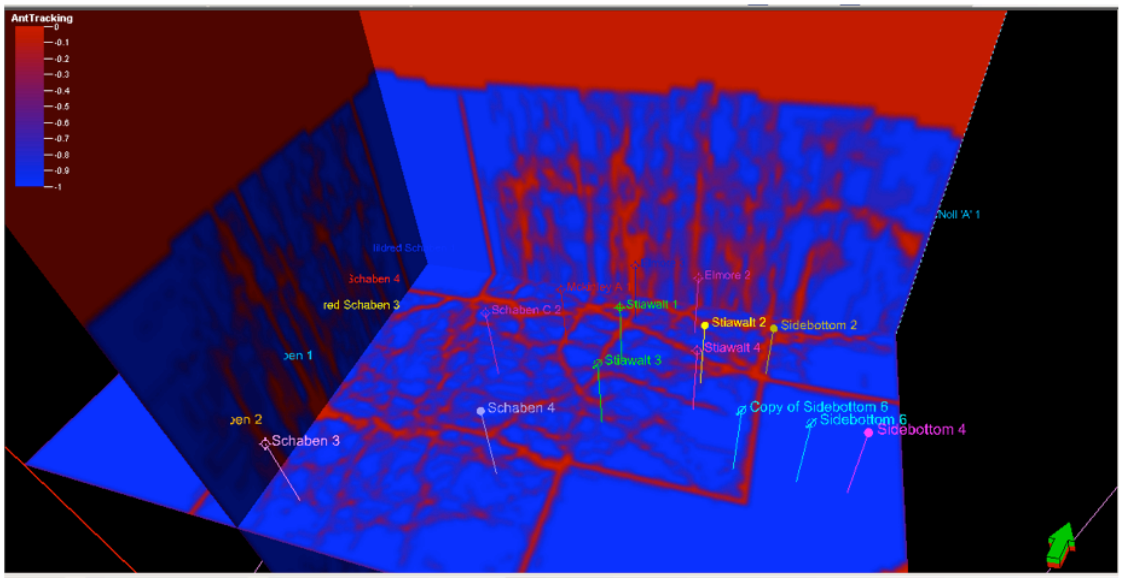

Figure 1-4a. Lineations traced from Passive ANT volume showing vertically confined and unconfined features (vertical exaggeration 10:1). Depth slice is at -2050 ft TVDSS, at Gilmore City level near the bottom of the Osage deep saline aquifer.

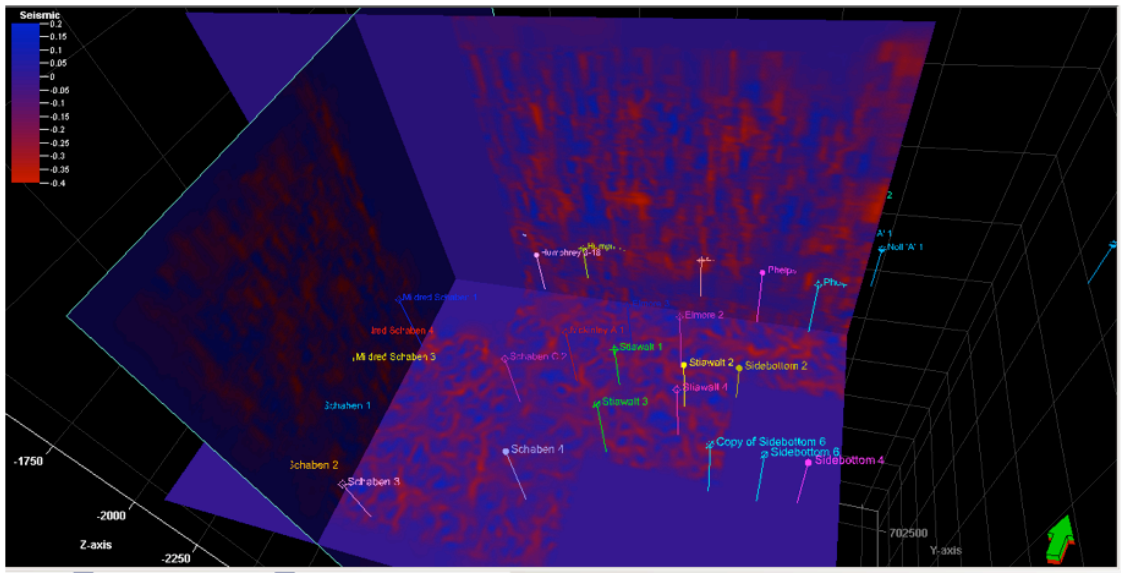

Figure 1-4b. Maximum negative curvature features showing less vertical connection than the ANT volume. Same view and scale as Figure 1-4a.

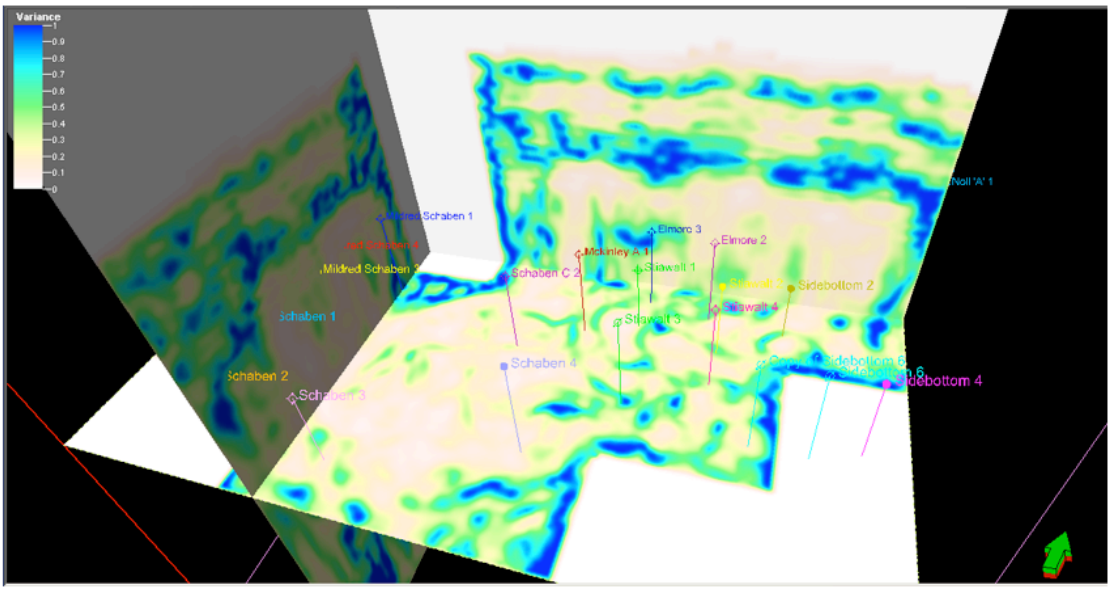

Figure1-4c. Chaos attribute volume showing more confined features than unconfined features. Same view and scale as Figure 1-4a.

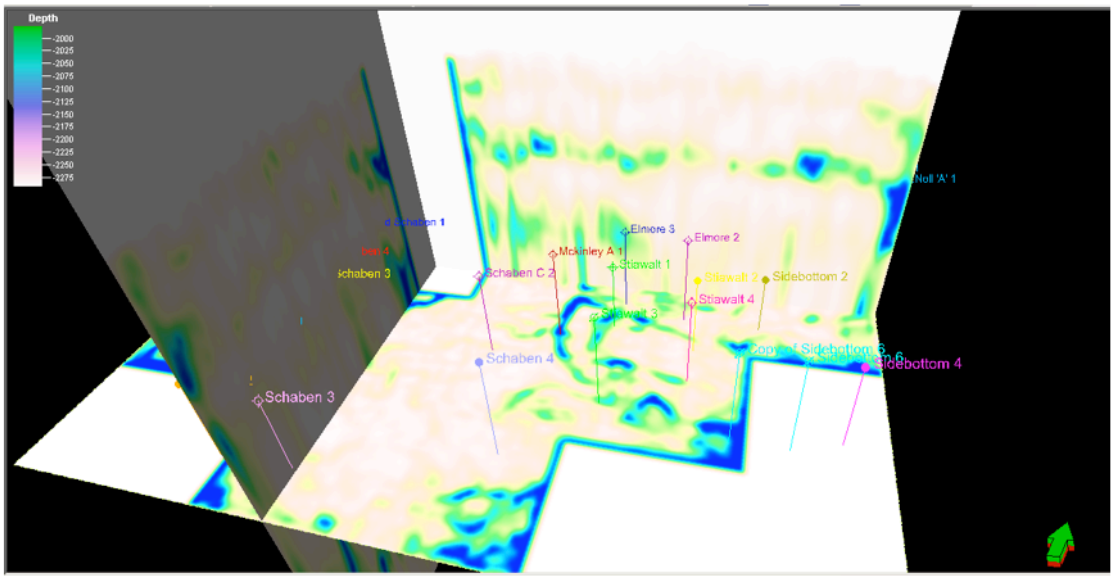

Figure1-4d. Features from Variance attribute volume showing few confined and unconfined features. Same view and scale as Figure 1-4a.

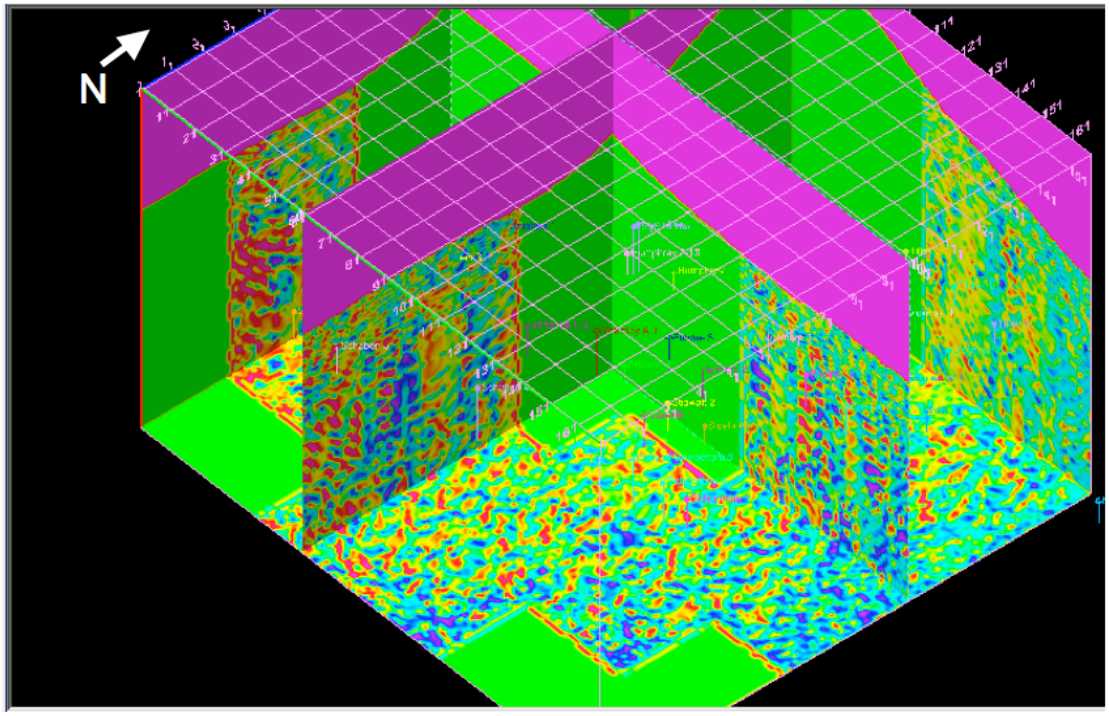

Figure 1-4e. Structural azimuth attribute volume with depth slice (-2159 FT TVDSS, below the Gilmore City unconformity), showing mainly confined features that may give clues to the fault and fracture framework. Only a few significant unconfined lineations are visible.

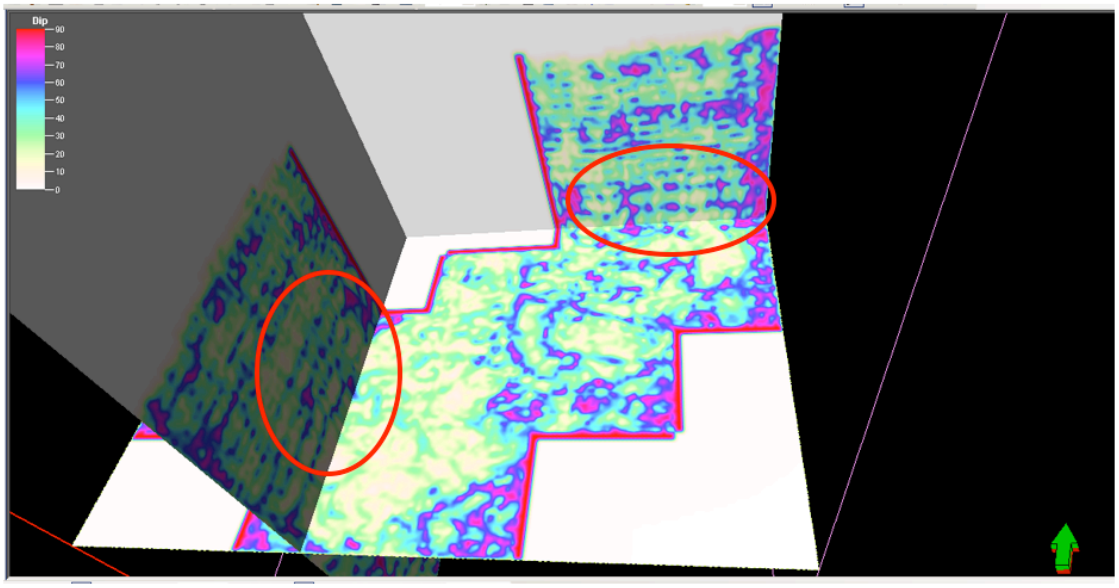

Figure 1-4f. Structural dip attribute volume with depth slice (-2050 FT TVDSS, base of saline aquifer) showing few vertical features penetrating from top to the base of the target beds. Most high angle features seem to be confined (e.g., as shown in the red circles).

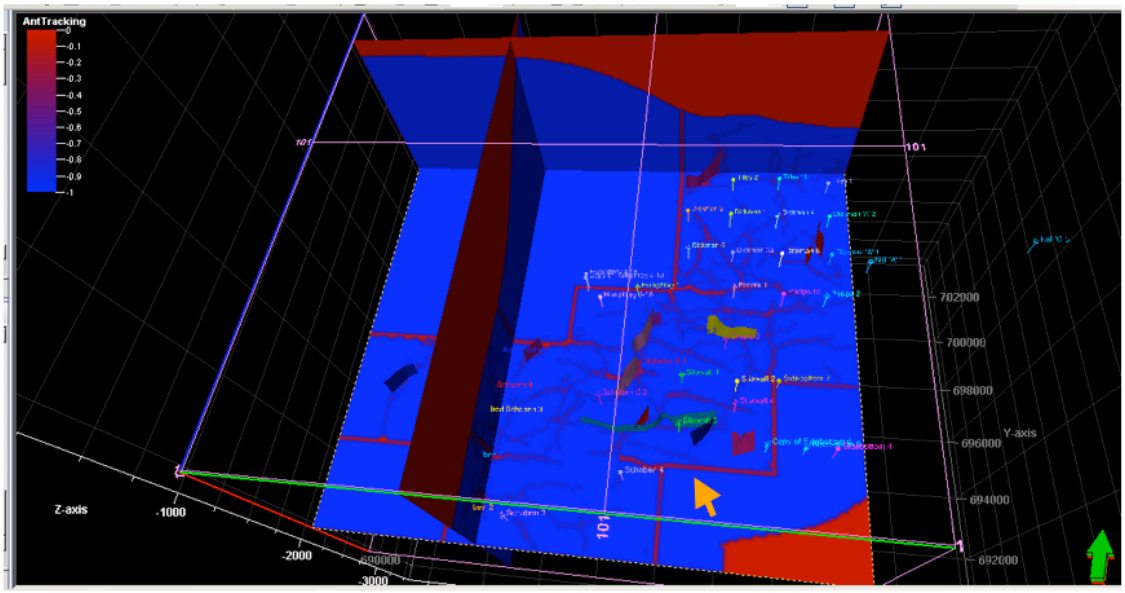

Figure 1-5a. Passive ANT volume (vertical exaggeration 5:1, Red=high_value, Blue=low_value). As viewed from vertical sections, linear features revealed by ANT are unconfined. Extreme high ANT values shown by thick dark red straight lines (orange arrow) are survey boundaries, and are eliminated while extracting fault planes. A few faults hand-picked from seismic lines are plotted for a comparison.

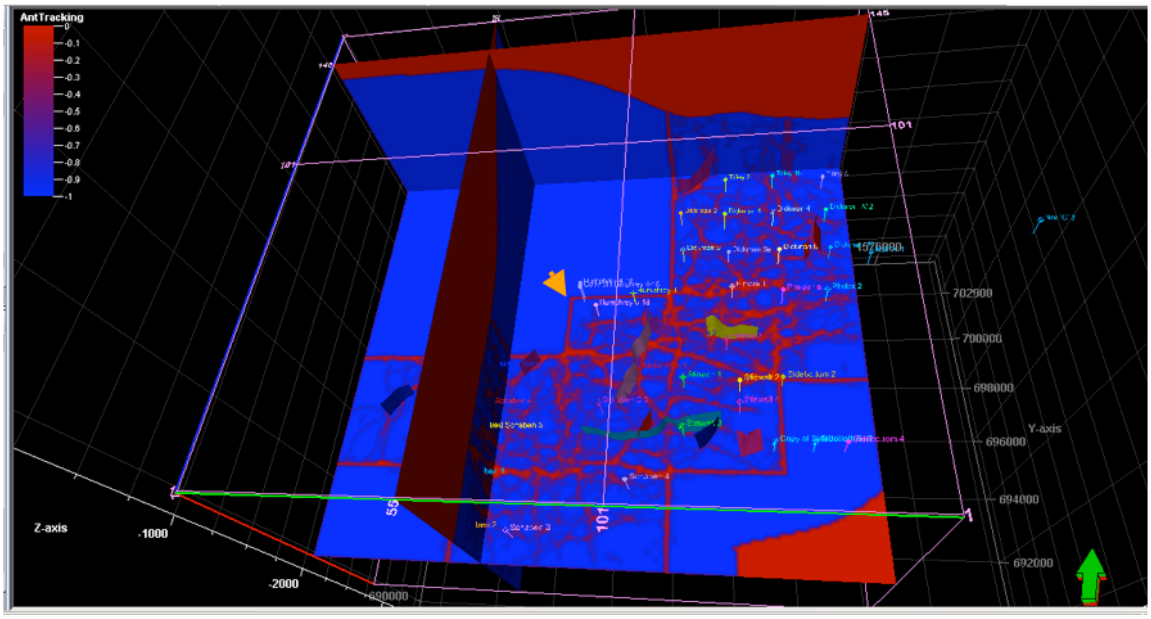

Figure 1-5b. Aggressive ANT volume (same scale, color scheme, and comments as 1-5a).

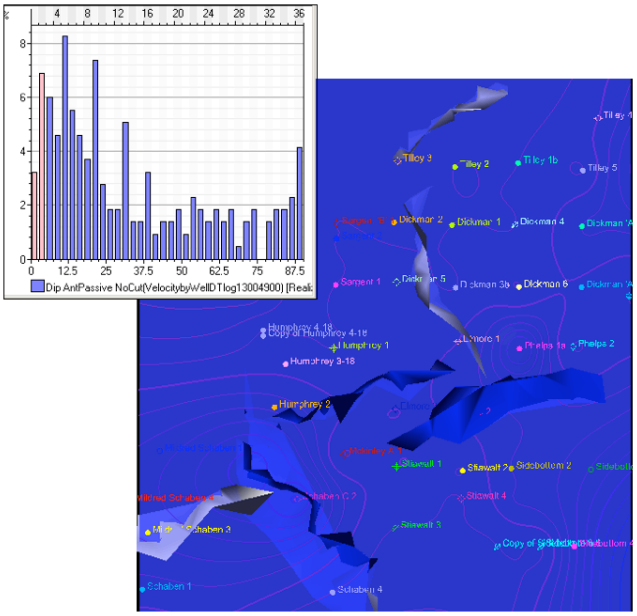

Figure 1-6a. Selected Planes Extracted from the Passive ANT Volume All planes with dips > 5°are shown by the blue bars in the histogram to left. The blue surface to the right with contours is the OWC. Most of the extracted planes were eliminated by the five factors described in the text and therefore not shown. The Passive ANT revealed four NE features and two NW features. Scale is 1:1.

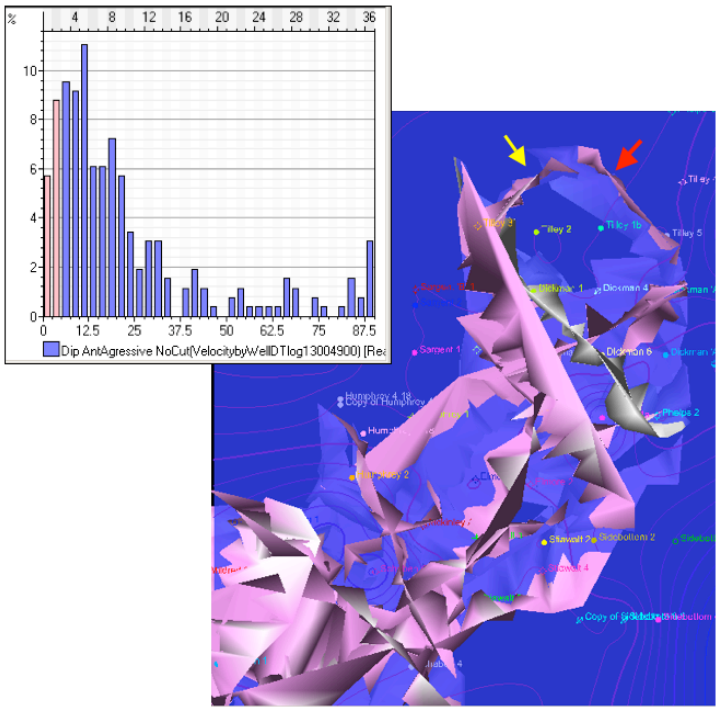

Figure 1-6b. Selected Planes Extracted from the Aggressive ANT Volume. All planes with dips > 5° are shown by the blue bars in the histogram to left. The NW plane (red arrow) is 4000 ft long and the NE plane (yellow arrow) is 2000 ft long. Scale is 1:1.

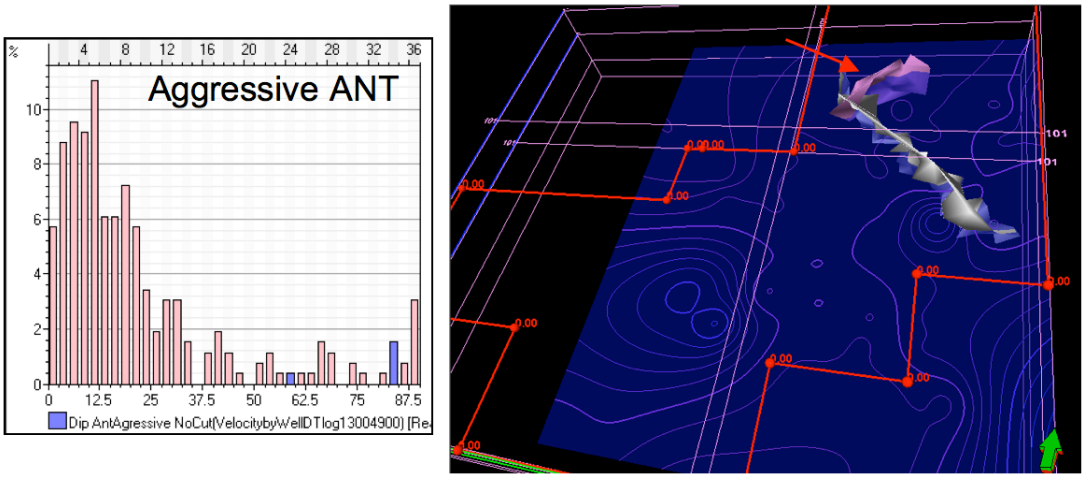

Figure 1-7a. Extracted ANT planes with dip > 60° (vertical scale 1:1). Blue bars in the histogram correspond to the two planes shown. More than 80% of the planes extracted from the Passive ANT volume and more than 90% of the planes extracted from the Aggressive ANT volume are with dips less than 30°. Length of NE Boundary Fault (red arrow) is about 2000 ft. OWC shown in blue.

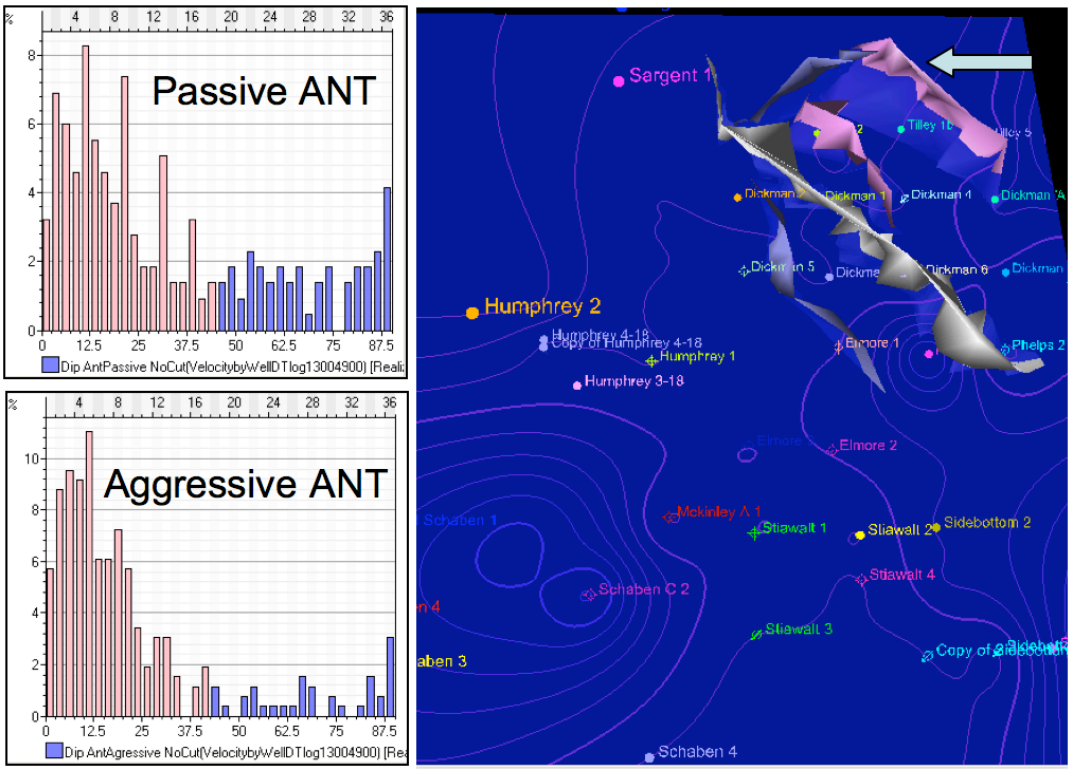

Figure 1-7b. Extracted ANT planes with dip > 45°. One 4000 ft long NE plane (arrow) was extracted from both passive and aggressive ANT volumes.

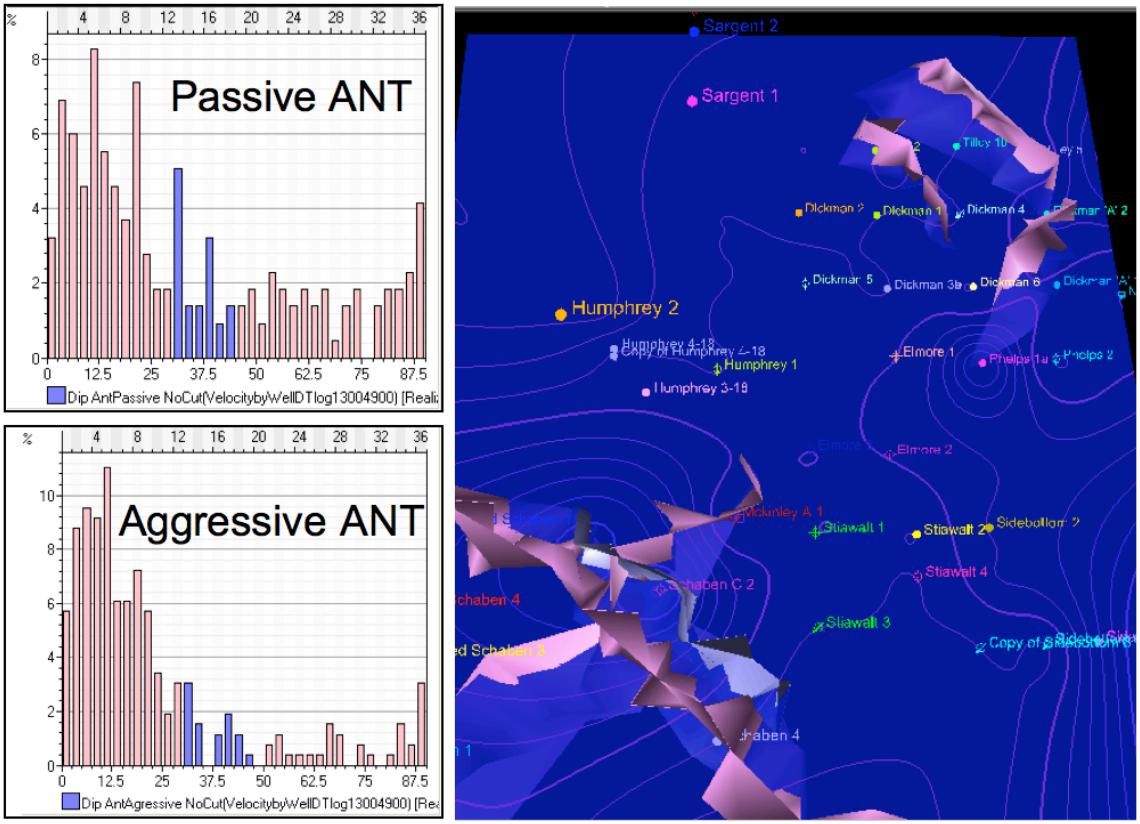

Figure 1-7c. Extracted planes With 30-45° dips (blue bars in histograms). Most planes were eliminated by the five criteria in the text. More NW than NE planes are in this dip range.

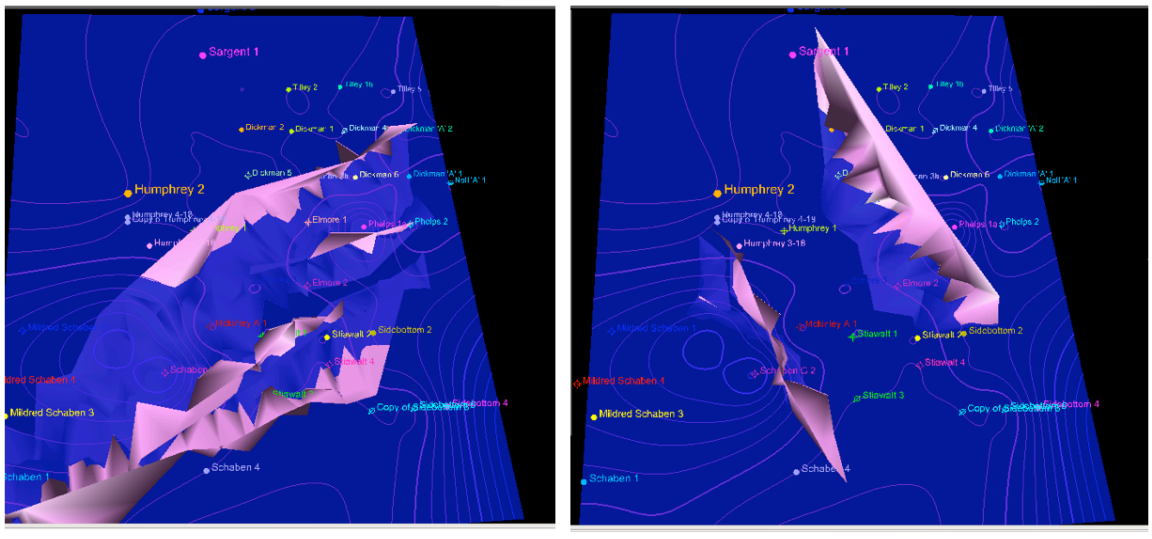

Figure 1-7d. Extracted ANT planes with 15-30° dips. Left: NE trending planes; Right: NW trending planes.

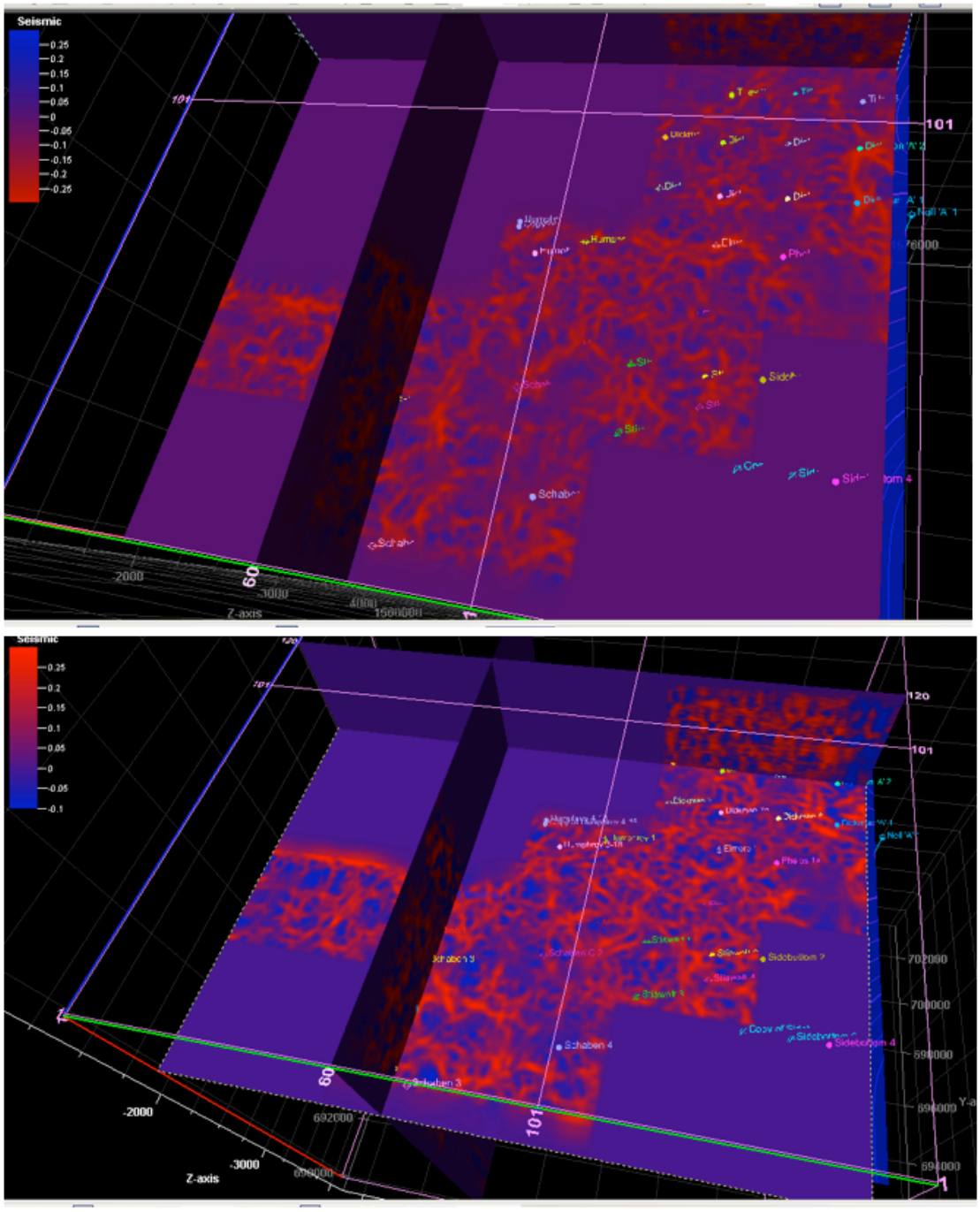

Figure 1-8a. Curvature attributes at -1860 ft TVDSS (Fort Scott level). Upper: Maximum negative curvature. Lower: Maximum positive curvature. Color convention used makes convex (arched) areas red in both maps. Vertical exaggeration 5:1.

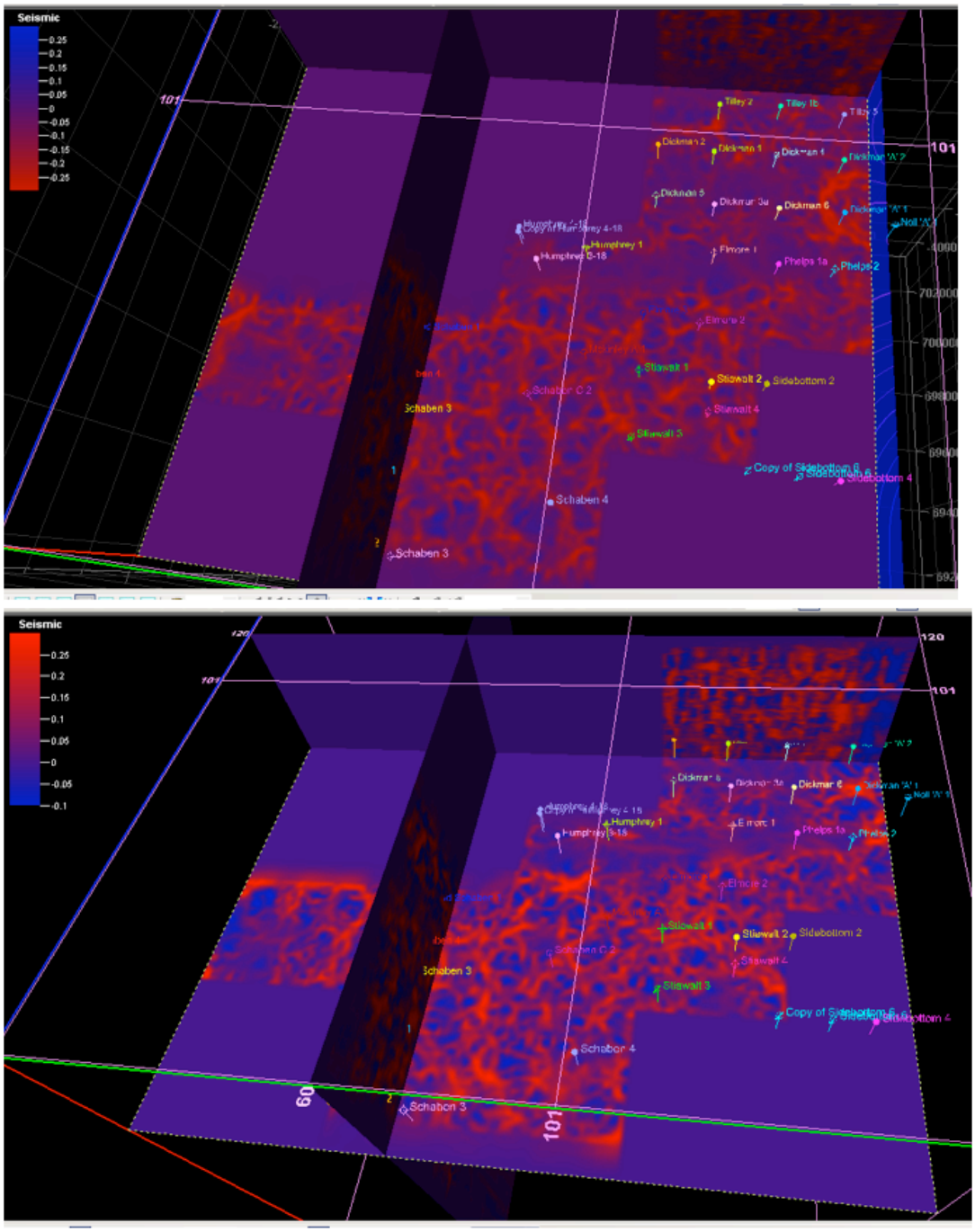

Figure 1-8b. Mississippian level curvature slices (-1960 TVDSS, about 15-20 ft above the OWC). Upper: Maximum negative curvature. Lower: Maximum positive curvature.

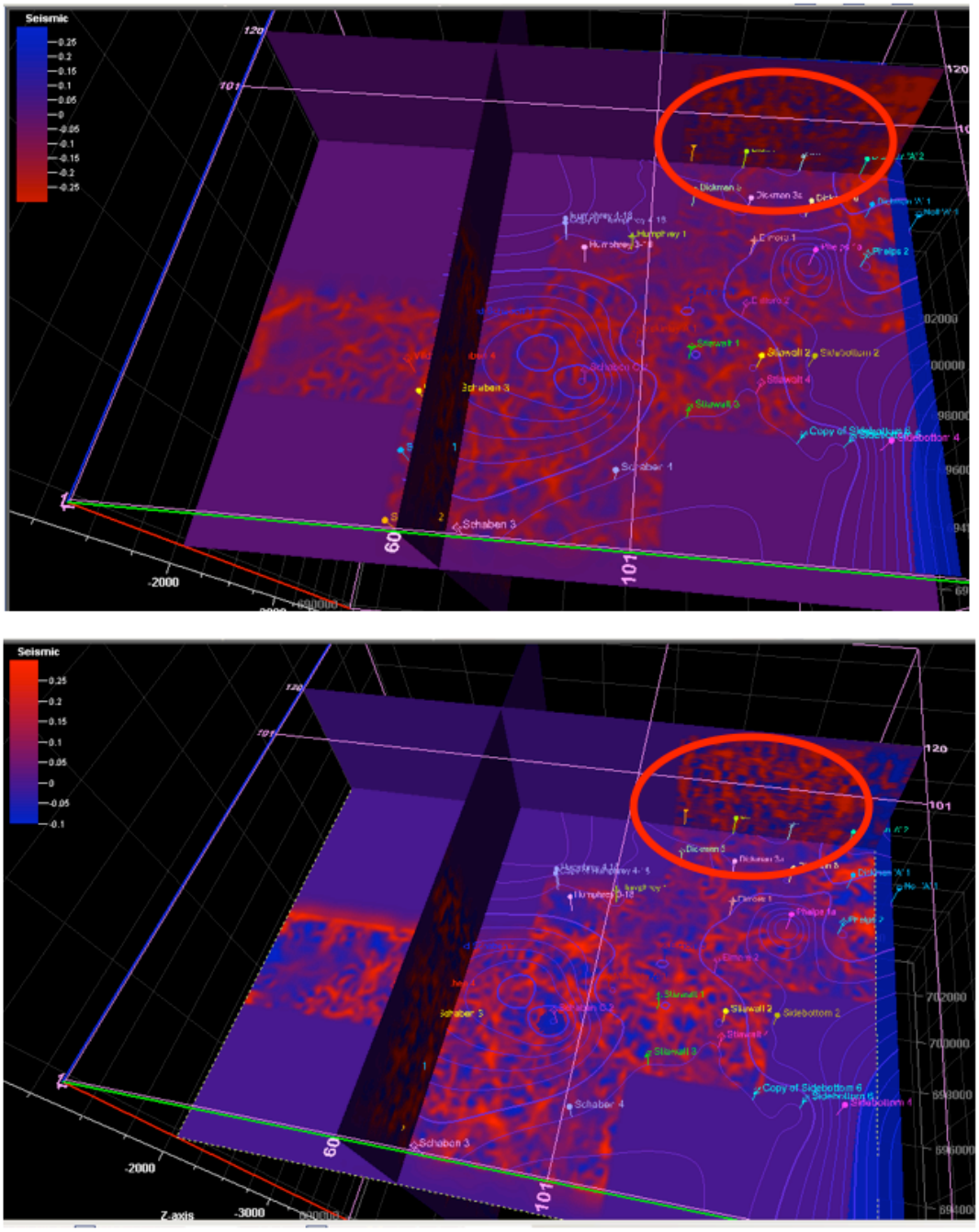

Figure 1-8c. Curvature attribute sliced at the oil-water contact (-1981 TVDSS). Upper: maximum negative curvature. Lower: Maximum positive curvature. As viewed from vertical intersections (red circle), the features are not vertically penetrating the strata. In plane view, they are much less linear and the distribution pattern does not match faults revealed by ANT and Chaos volumes.

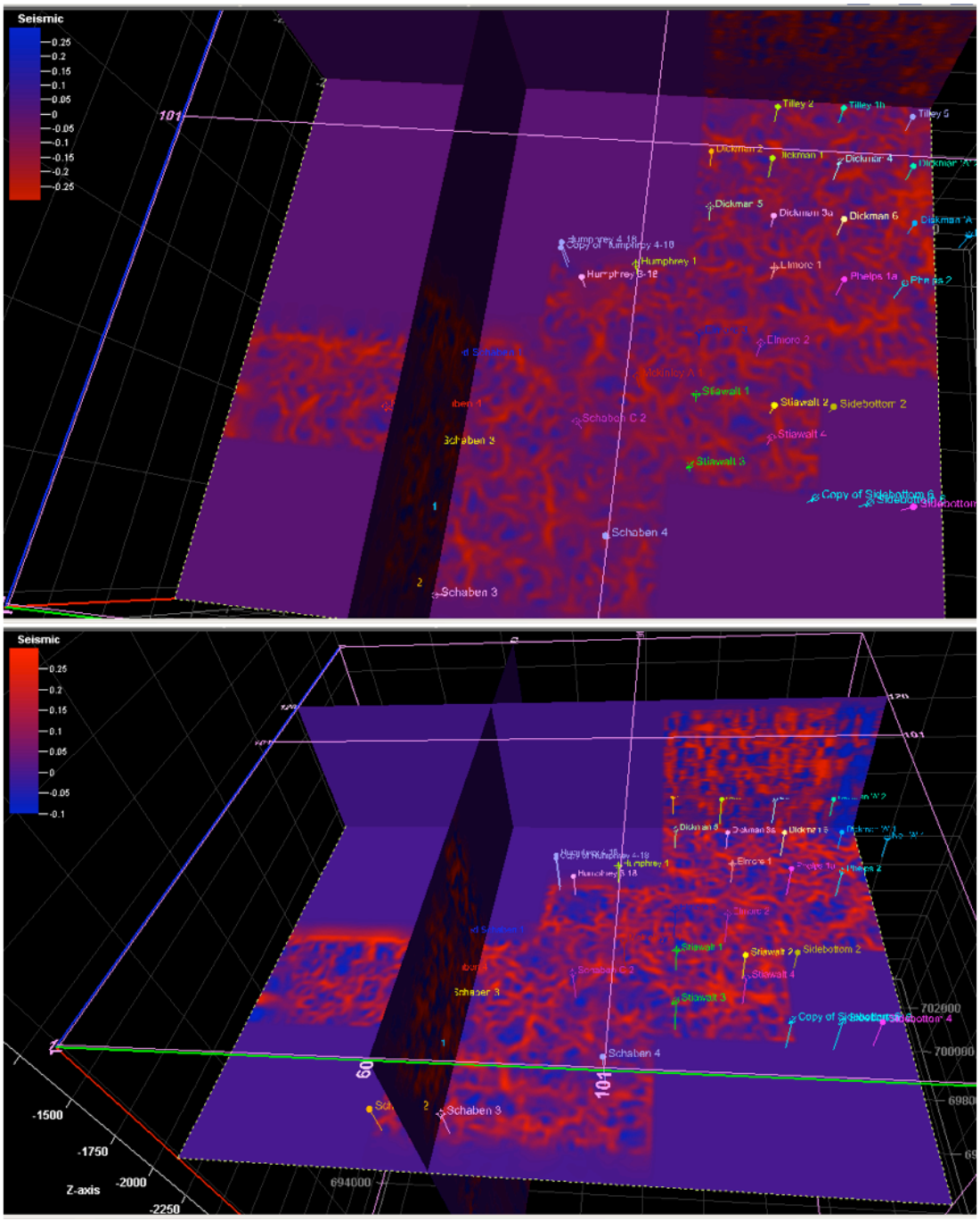

Figure 1-8d. Curvature attributes at Gilmore City level (-2050 TVDSS, near base of deep saline aquifer). Upper: Maximum negative curvature. Lower: Maximum positive curvature.

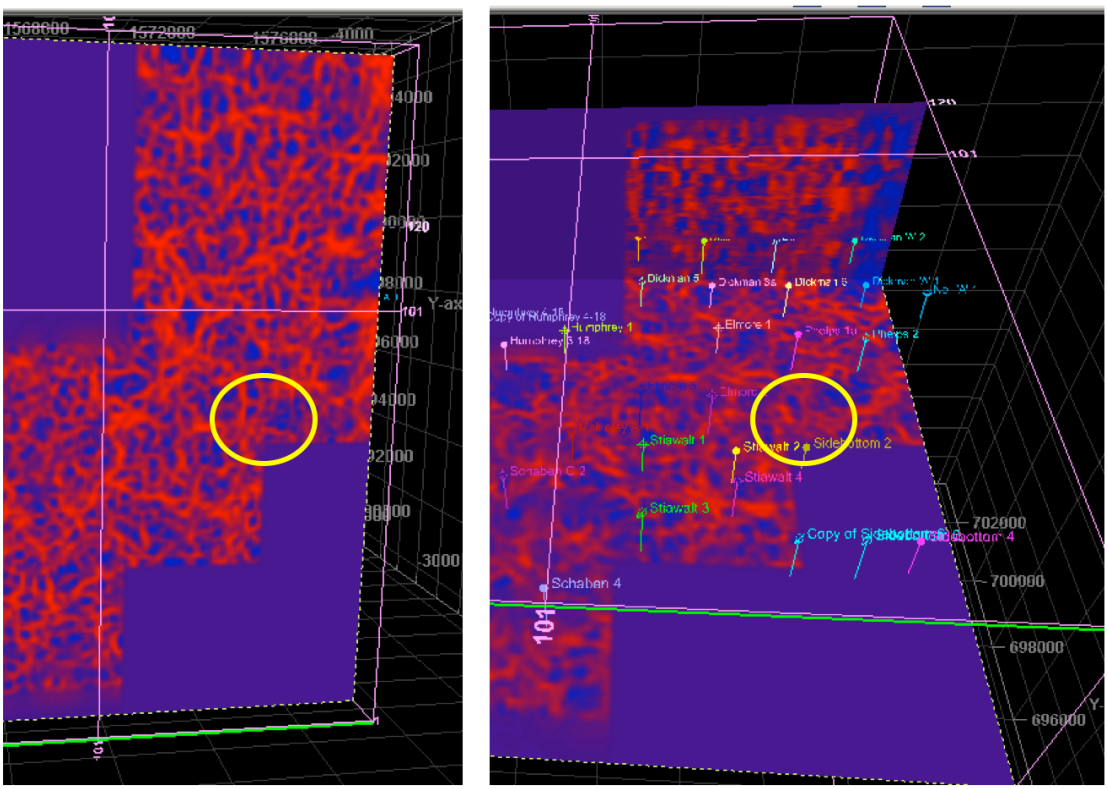

Figure 1-8e. Curvature comparison with depth. Maximum positive curvature slices at -1500 TVDSS (left: above the Fort Scott), and at -2050 TVDSS (right: base of deep saline aquifer). Concave areas are blue for both maps (vertical exaggeration 5:1). The shallow pattern is more complicated indicating features are confined (not vertically penetrating through the entire strata).

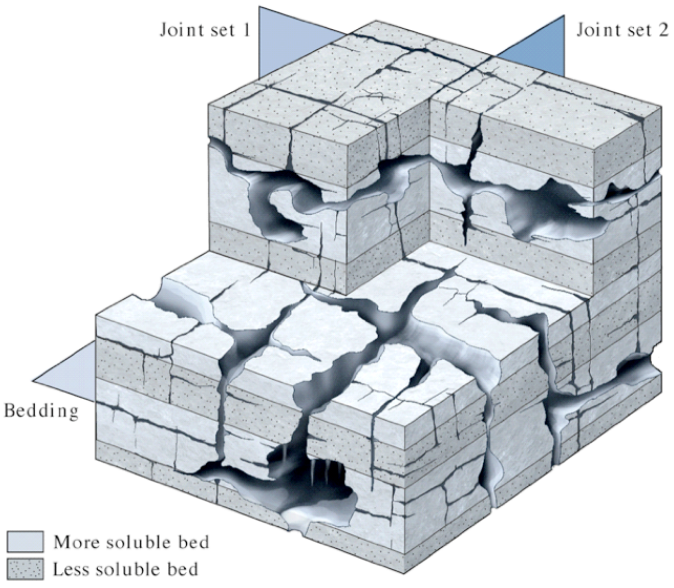

Figure 1-8f. Conceptual model of karst development in carbonates (from Marshak, 2001).

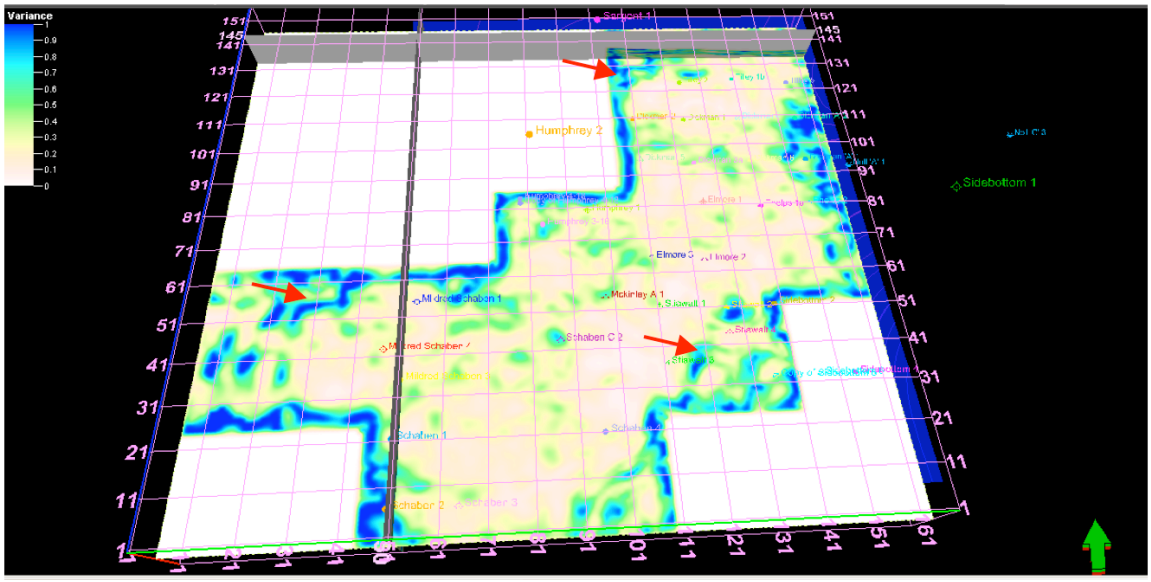

Figure 1-9a. Chaos attribute slice at Fort Scott level (-1860 TVDSS). Blue indicates more chaotic, less predictable, data. Chaos is low at this level, except at several possible NE faults (red arrows) and high values at survey boundaries.

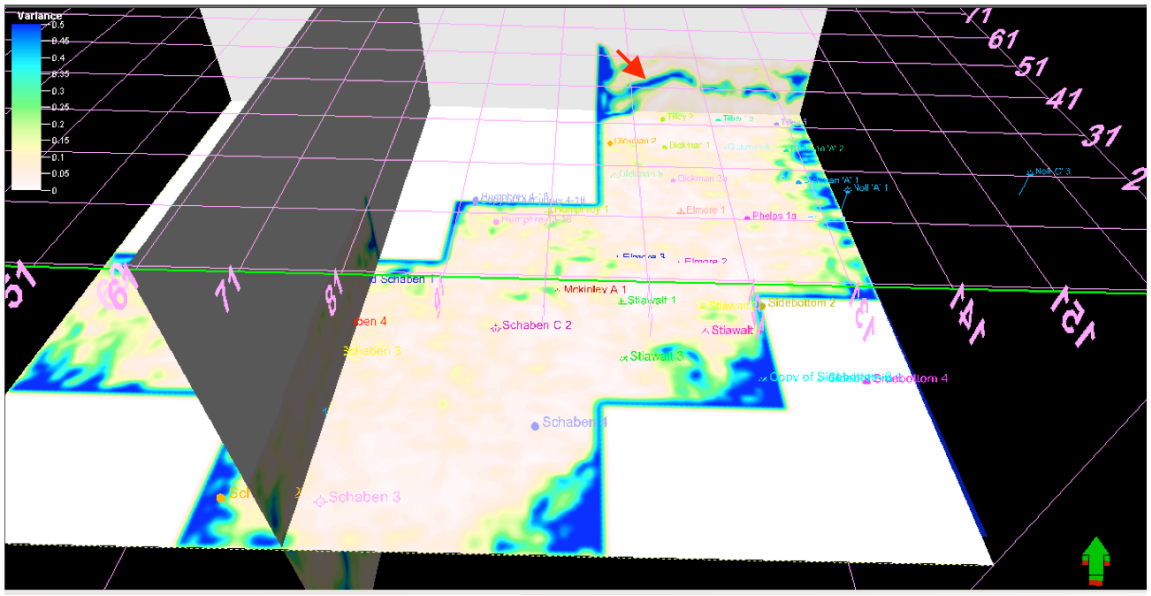

Figure 1-9b. Variance attribute slice at Fort Scott level (-1860 TVDSS). As with chaos, deviates from low values only along major faults and survey boundaries.

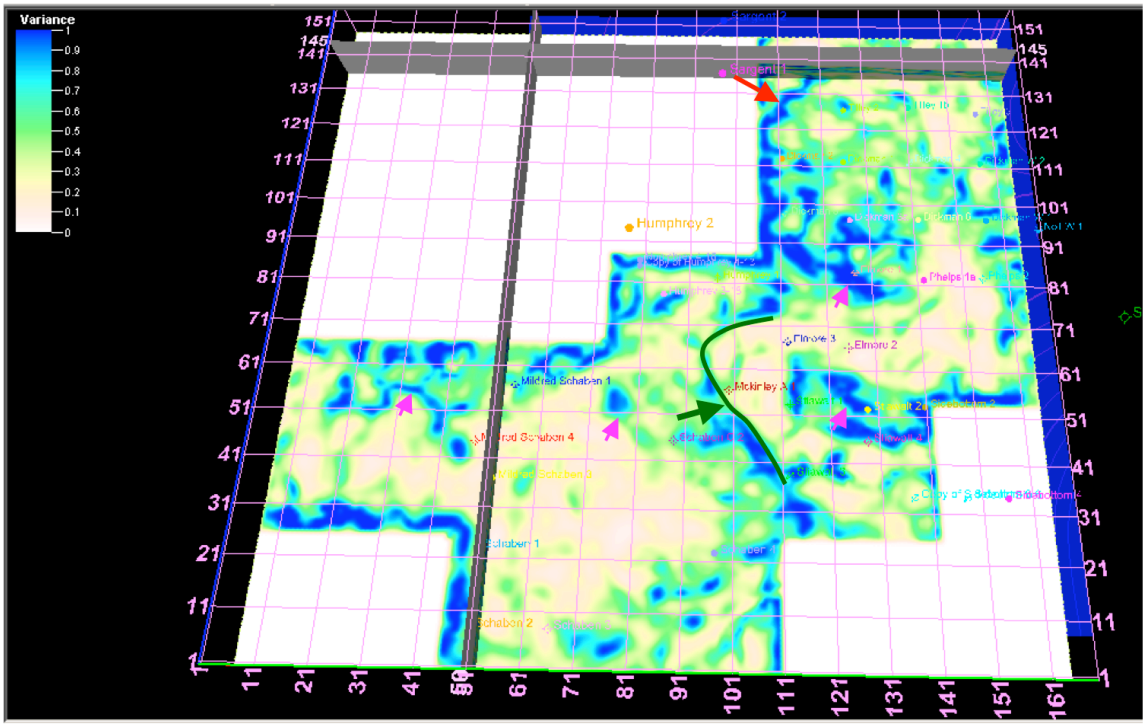

Figure 1-10a. Chaos attribute slice at -1950 ft TVDSS (near the Mississippian unconformity). Complicated chaos patterns and more significant contrast between high and low chaos areas than at the Fort Scott level. The green arrow and line indicates the channel bend, in addition to the NE and NW fault (red and pink arrows).

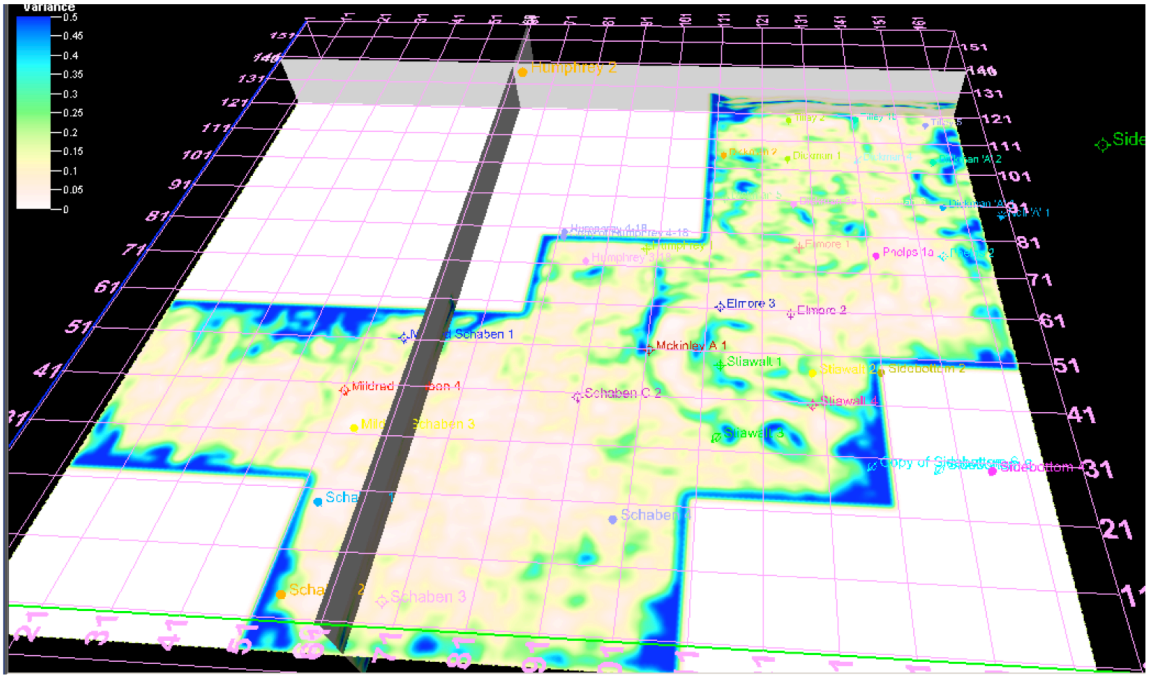

Figure 1-10b Variance attribute slice at -1950 ft TVDSS (near Miss. Unconformity). Variance is relatively high at this level compared with at Fort Scott, similar to the chaos pattern.

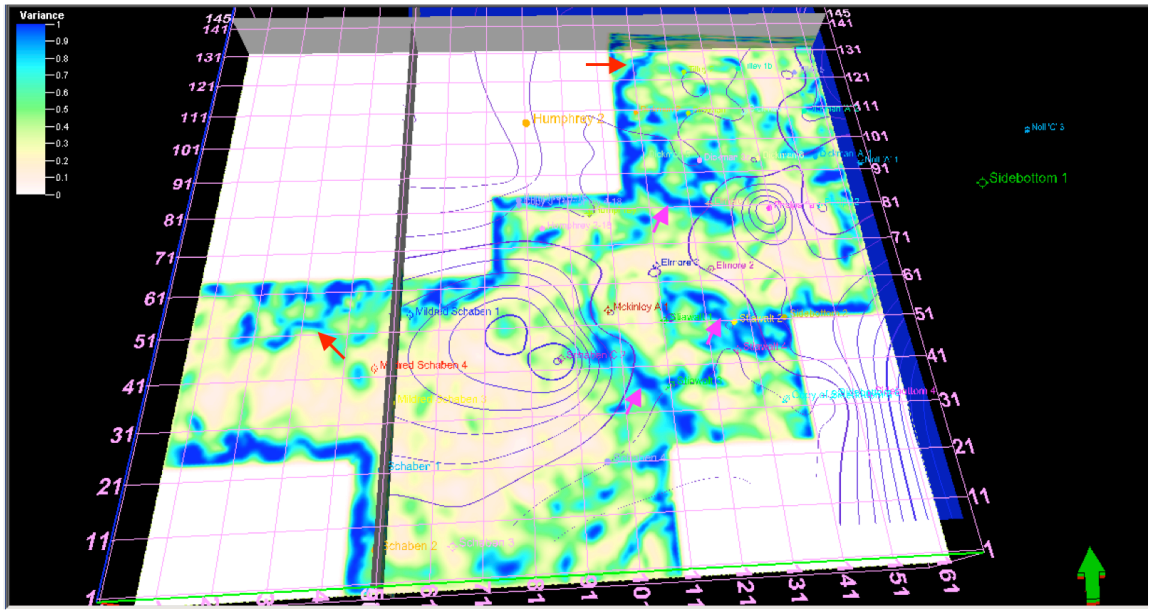

Figure 1-11a Chaos attribute slice at -1971 ft TVDSS (slightly above the OWC within the Mississippian carbonate reservoir). The OWC is shown by the purple contour lines on white background. The pattern of chaos is complicated, with laterally connected NE (red arrows) and NW (pink arrows) patterns. The contact between high and low chaos areas, however, is less significant than seen near Mississippian Unconformity.

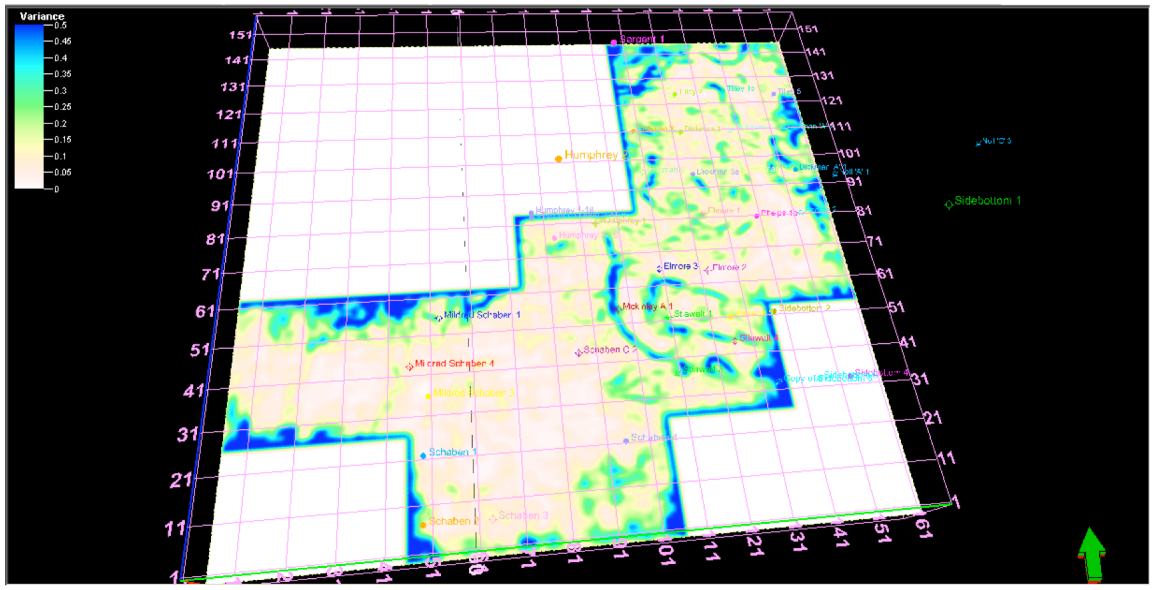

Figure 1-11b. Variance attribute slice at -1981 ft TVDSS (oil-water contact).

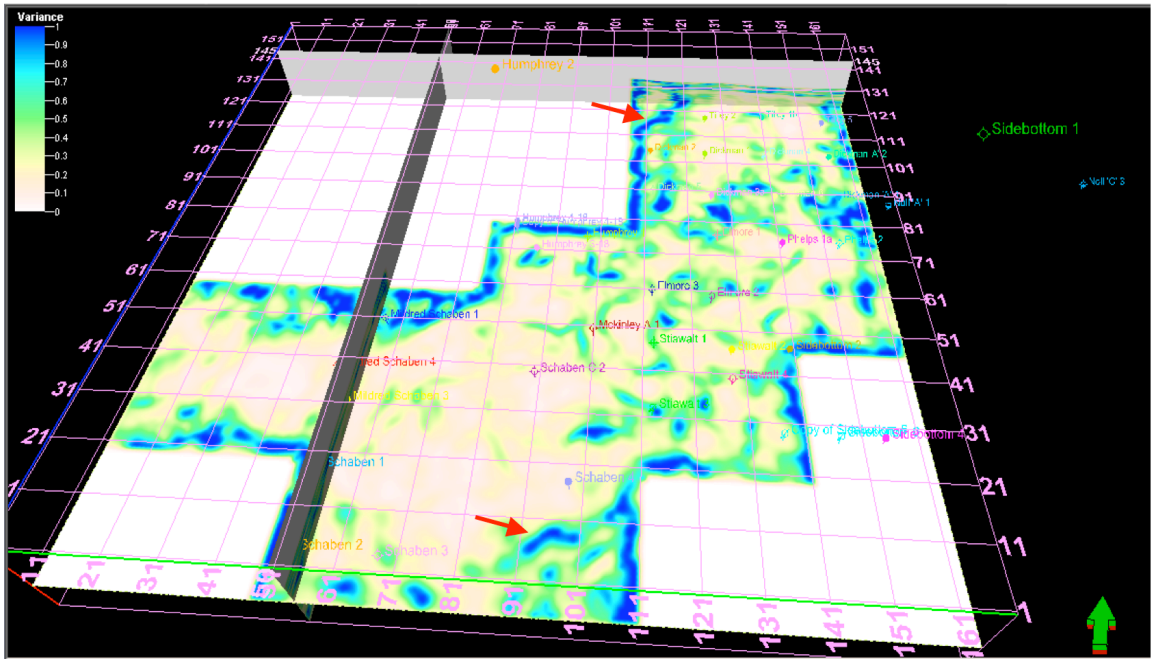

Figure 1-12a. Chaos slice at -2050 ft TVDSS (Gilmore City level). The chaos pattern at this depth is less complicated with less connectedness than near the Mississippian unconformity.

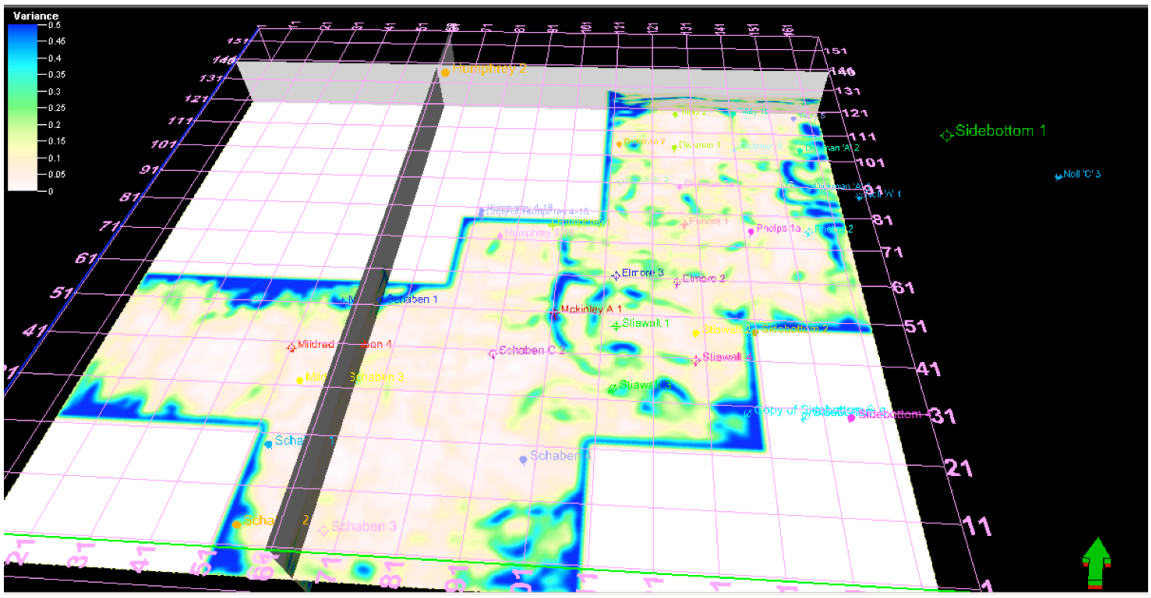

Figure 1-12b. Variance slice at -2050 ft TVDSS. The variance pattern at this depth is less complicate with less connectedness than the slice near Miss. unconformity. Features are mostly confined, isolated patches at this depth.

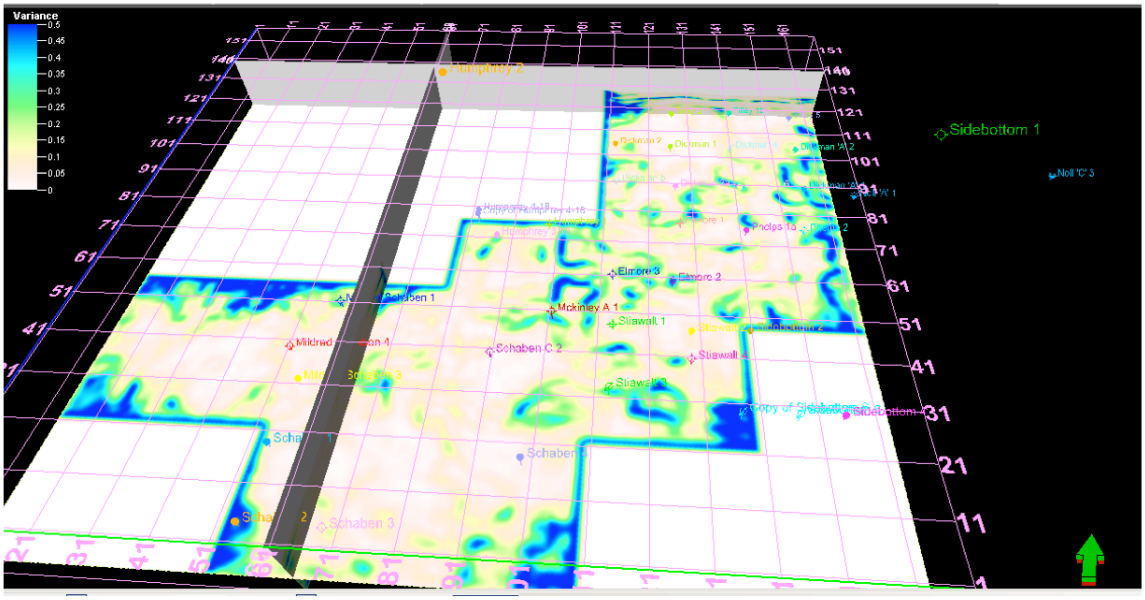

Figure 1-12c. Variance slice at -2150 ft TVDSS (below Gilmore City). The variance pattern at this depth is limited to isolated patches like sinkholes, mostly confined to certain surfaces. If they represent faults and other structures, they should be most complicated at this deeper level than in shallower, younger carbonate strata.

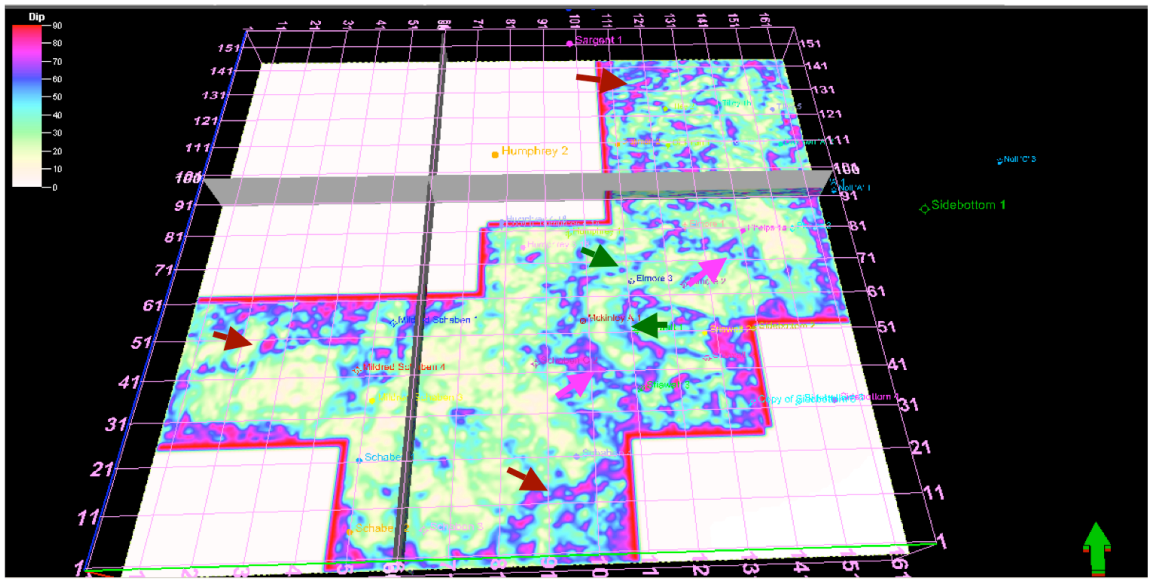

Figure 1-13a. Local structural dip attribute at -1981 ft TVDSS (oil-water contact). Some high-dip features are channel boundaries (green arrows). Many high dips trending NE or NW correlate with features revealed by ANT (red and pink arrows).

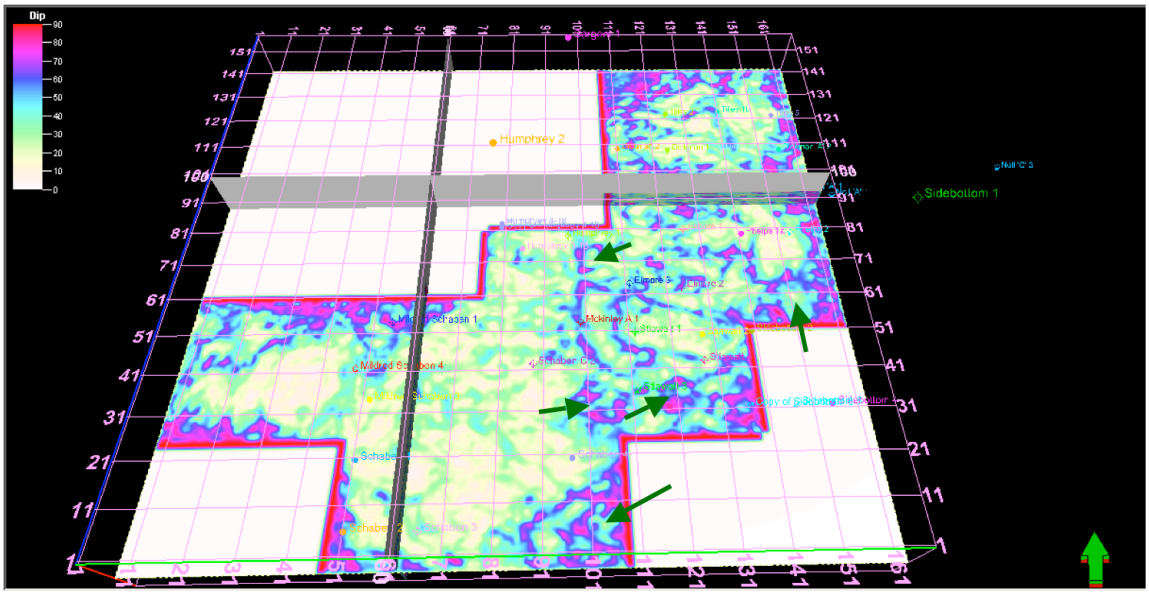

Figure 1-13b. Local structural dip attribute -2040 TVDSS (saline aquifer level). The high dip features show some isolated round patches (red arrows) not clearly seen at shallower depth near OWC.

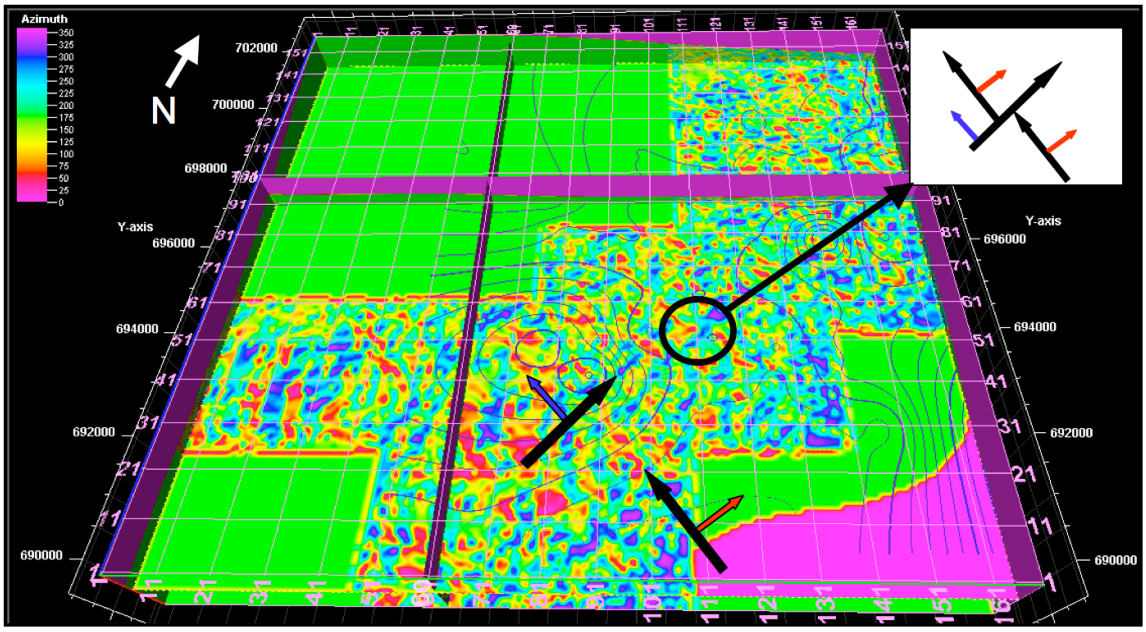

Figure 1-14a. Azimuth attribute slice at -1981 ft TVDSS (oil-water contact). Blue-Black arrow set represent an azimuth 310˚ (NW, blue arrow) feature aligned at 60˚ (NE, black arrow). The same color convention is used for the red-black arrow set. In the circled are, these two trends appear to intersect with and show offset as detailed in the inset sketch.

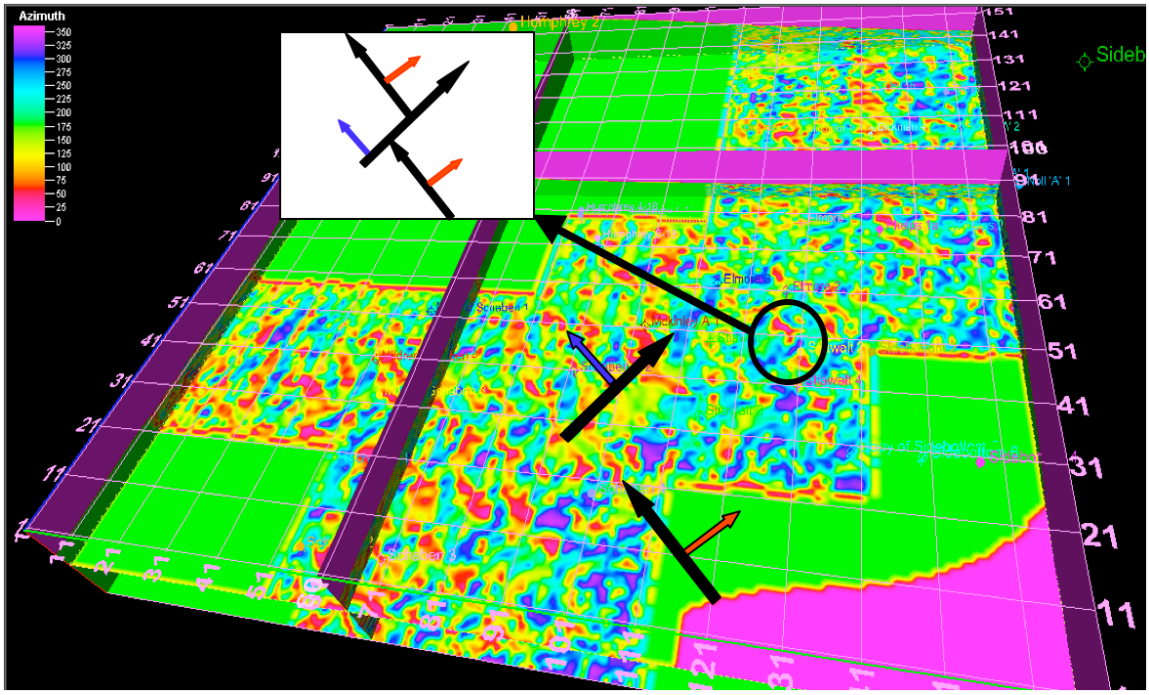

Figure 1-14b. Azimuth attribute slice at -2046 feet TVDSS (within Upper Osage saline aquifer). See Fig. 1-14a for explanation of arrows.

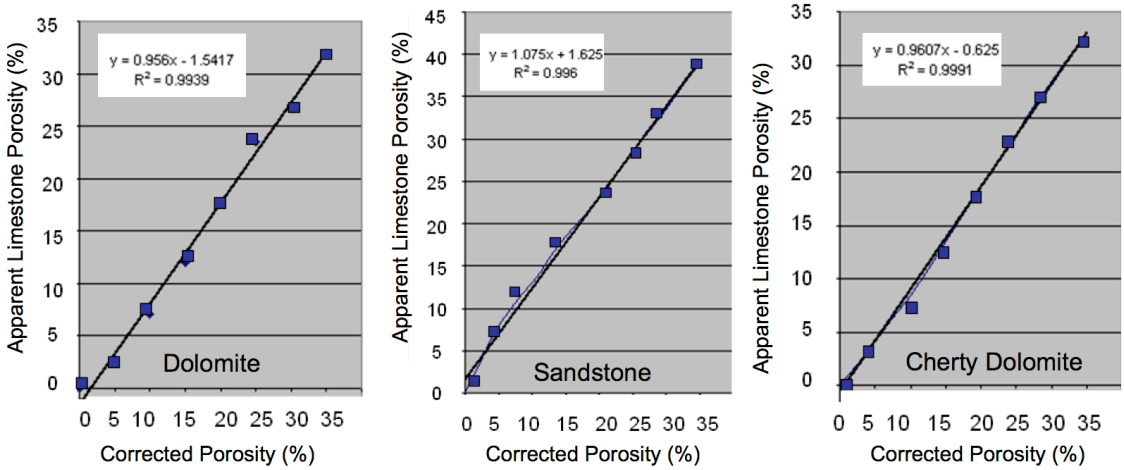

Figure 2-1. Correction plots and equations for adjusting apparent limestone neutron porosity to other lithologies.

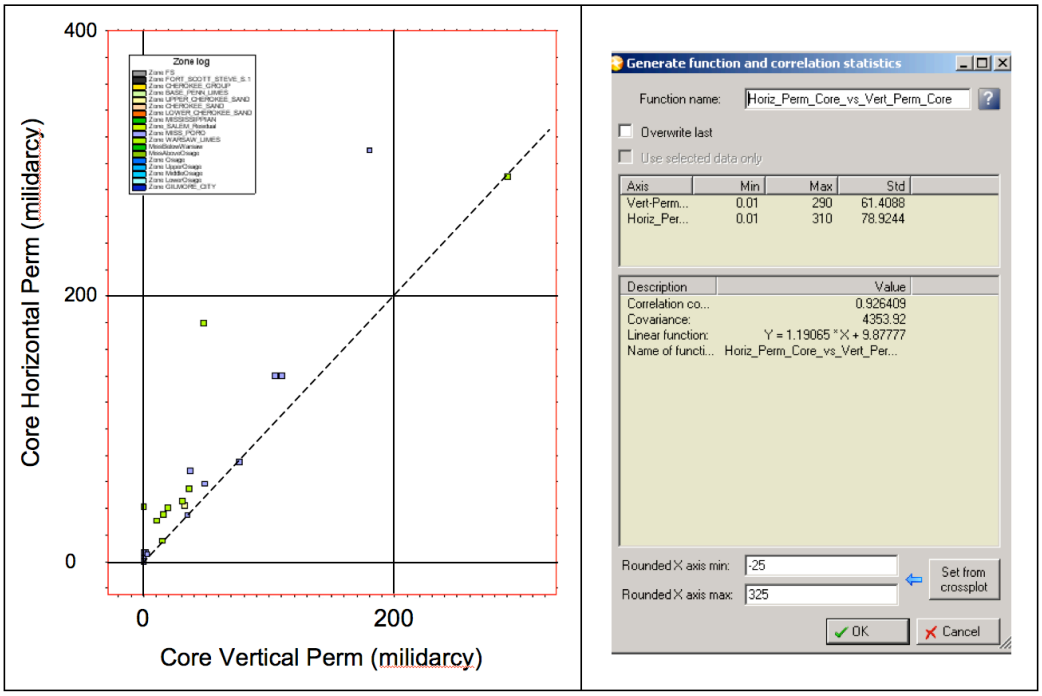

Figure 2-2a. Horizontal and vertical permeability from core measurements in Dickman 4 well. Horizontal permeability is generally higher than vertical by about 20%. Equality line is dashed.

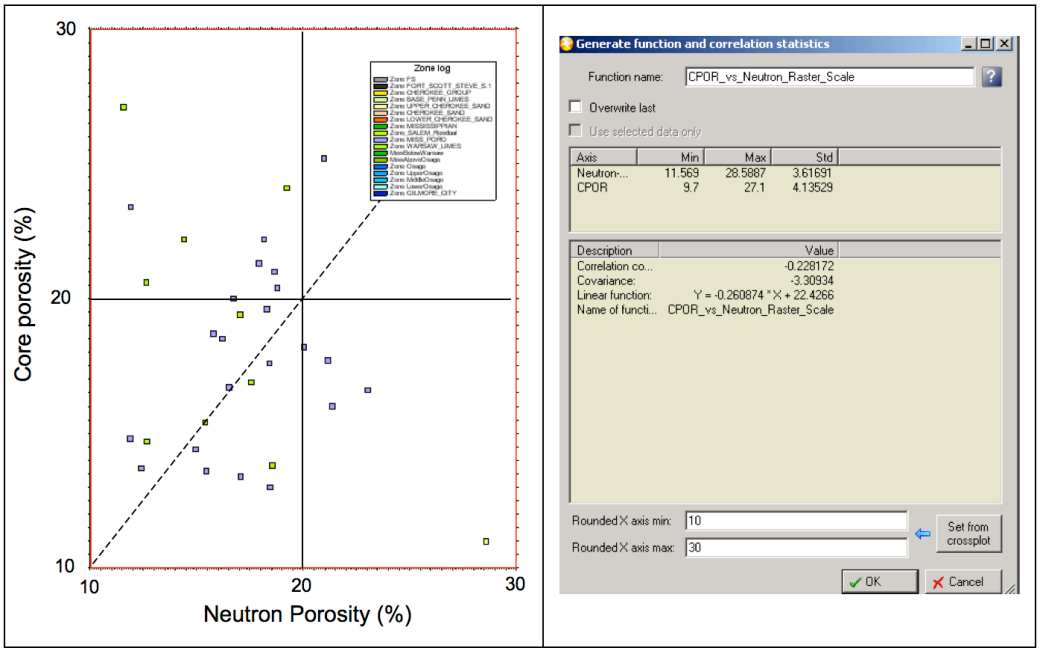

Figure 2-2b. Core vs. neutron porosity for shallow reservoirs in the Dickman 4 well. Although the correlation is low, this equation allows core porosity to be estimated from 17 litho-corrected neutron porosity logs for shallow reservoirs and used for permeability computation. Equality line is dashed.

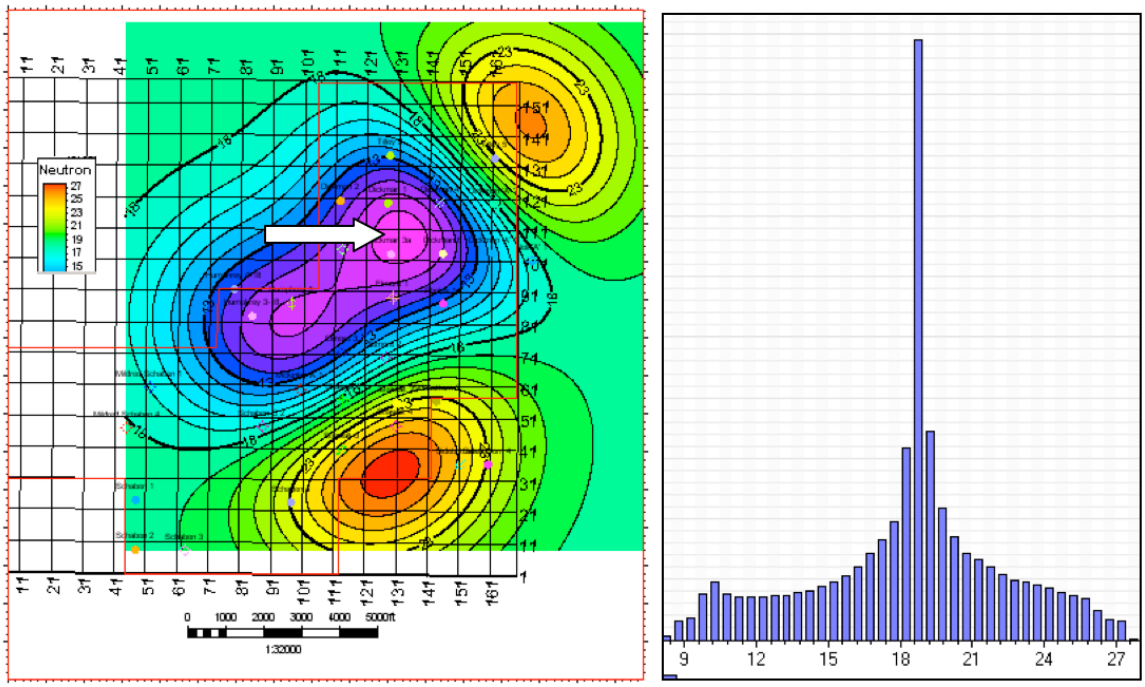

Figure 2-3a. Zone-averaged uncorrected neutron porosity for Fort Scott Limestone (N=18, peak 19%, minimum at arrow is 10%).

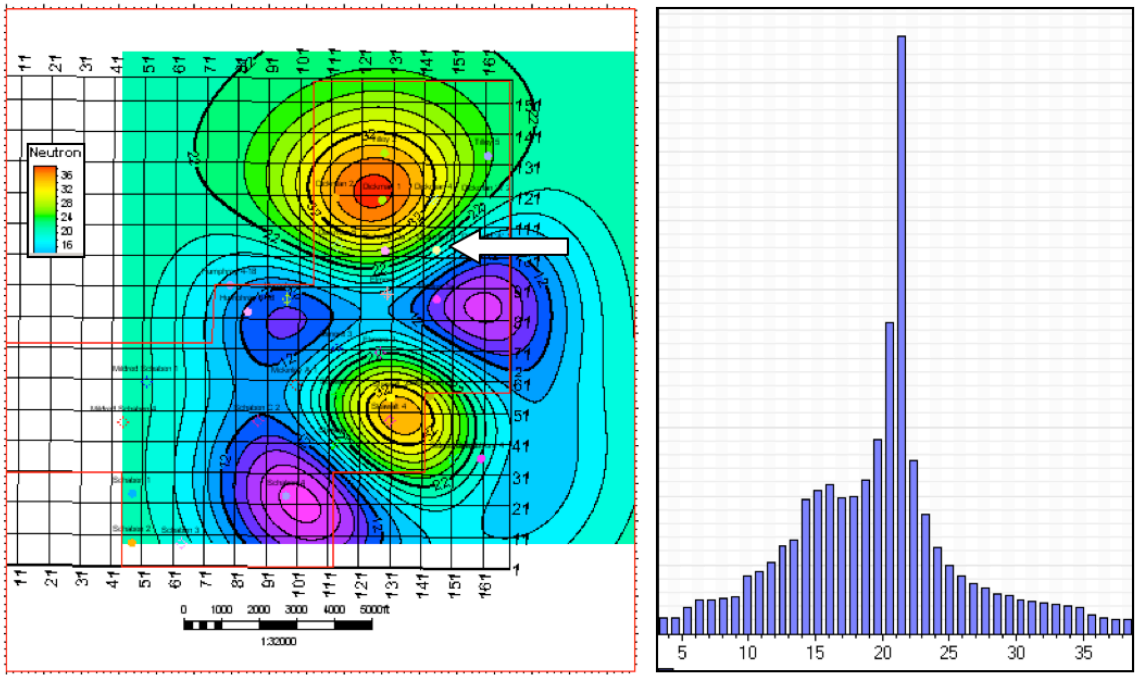

Figure 2-3b. Lower Cherokee uncorrected neutron porosity map (N=7, peak 21-23%).

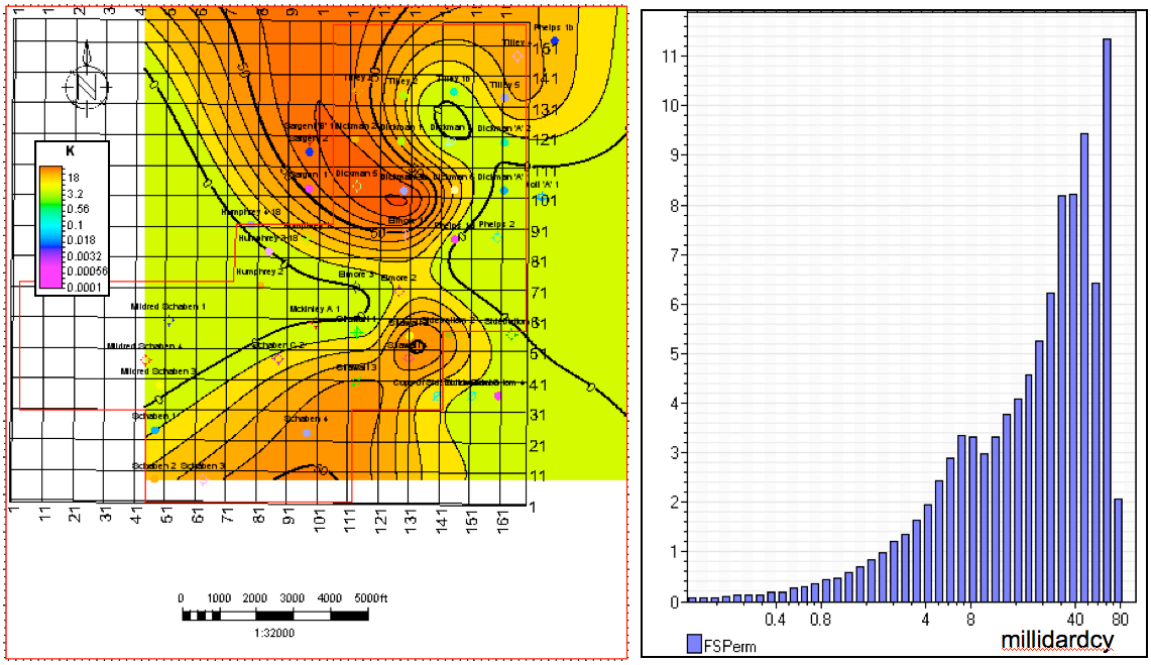

Figure 2-4a. Estimated zone-averaged permeability for Fort Scott Limestone (N=18).

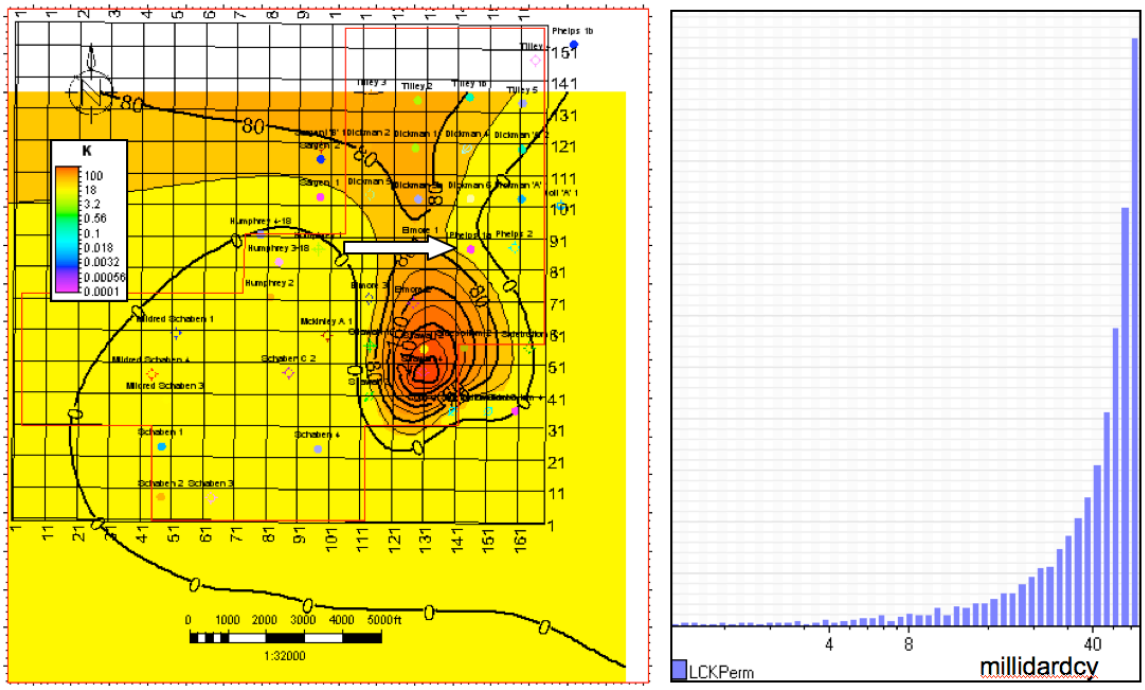

Figure 2-4b. Computed zone-averaged permeability for Lower Cherokee sandstone (N=7). Single available core measurement is 42 md. This interval may be productive in Phelps 1a well (arrow).

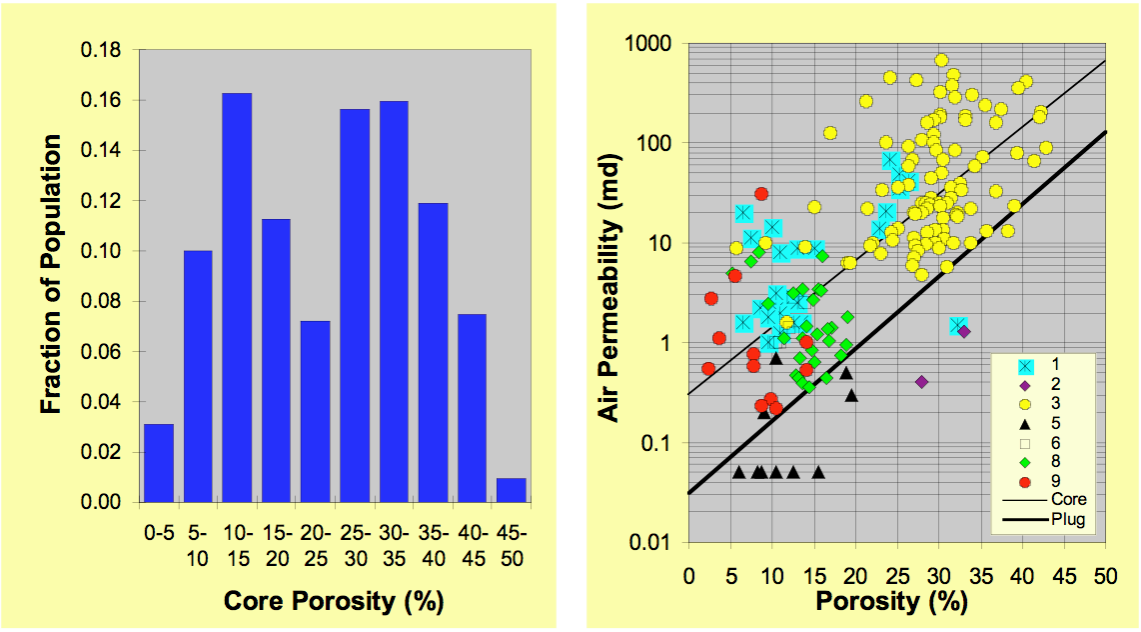

Figure 2-5. Regional characterization of the Mississippian Osage Chat in south-central Kansas based on 26 fields. Left: Core porosity histogram. Right: Core permeability vs. porosity from upper whole cores. The relationship derived from the cross-plot is: Log k =0.067*ϕ-0.53 where ϕ is whole core porosity (from Alan, Guy, and Watney, 2002).

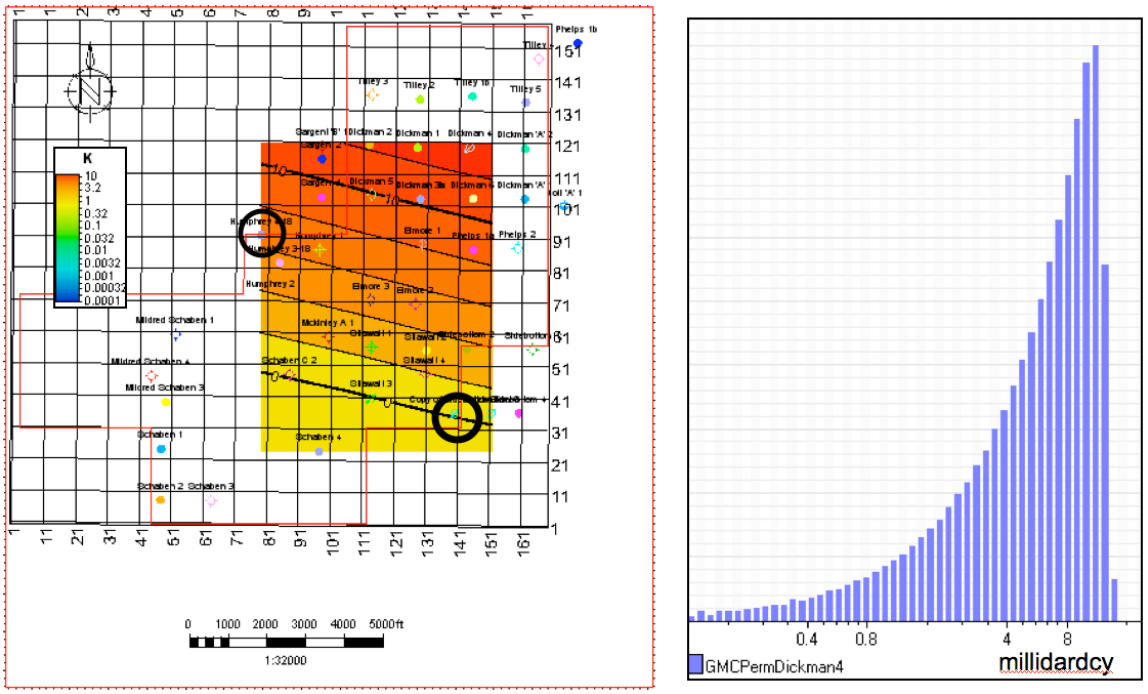

Figure 2-6. Estimated permeability for Osage deep saline aquifer based on the porosity-permeability relationship in Fig. 2-5. Only two data points (circles) contributed to the computation. The maximum computed value is 20 md.

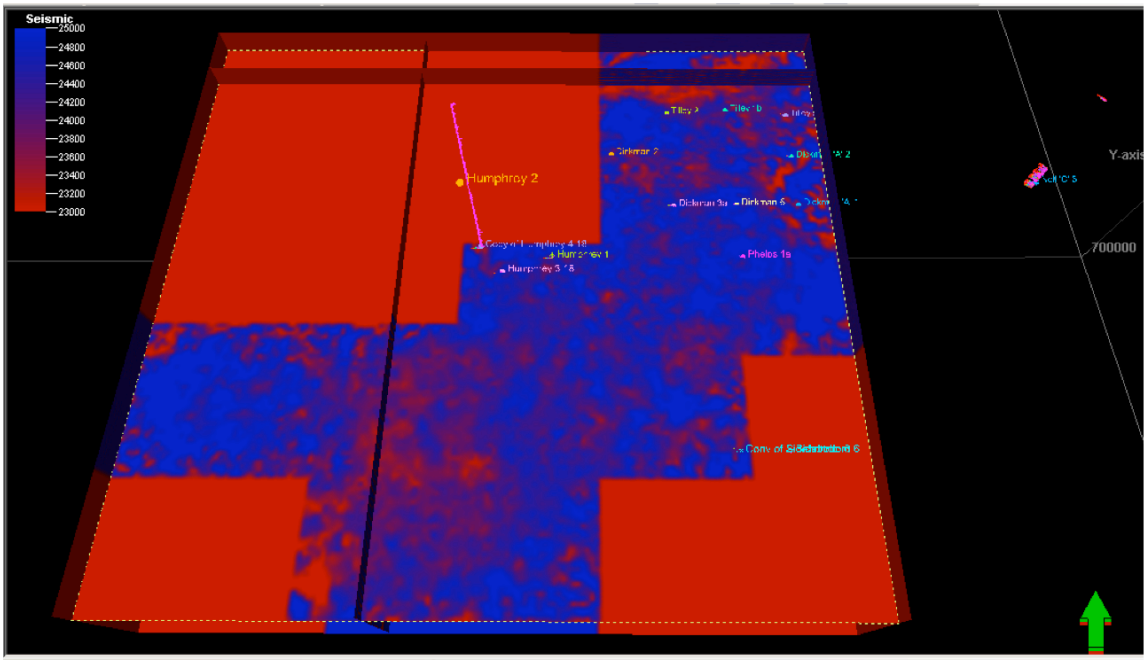

Figure 2-7. Seismic impedance volume slice at -1840 ft TVDSS (Fort Scott), near the top of the Dickman geological model. Red is low impedance, indicating softer, higher porosity rocks.

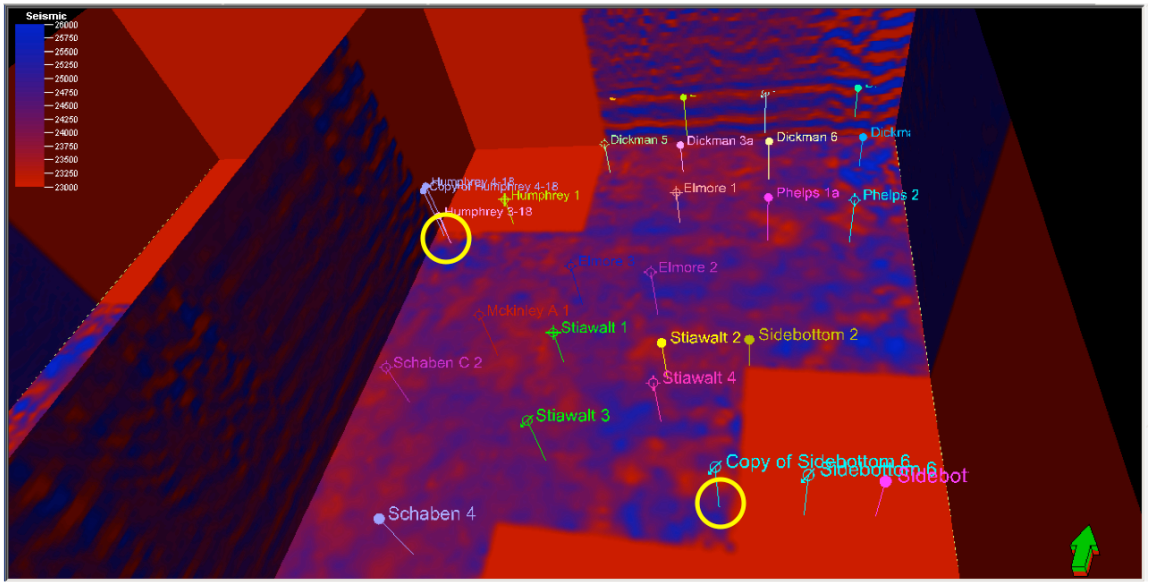

Figure 2-8. Depth-converted impedance volume slice at -2050 ft TVDSS (Gilmore City, below saline aquifer), near the base of the Dickman geological model. With only two well penetrations through the deep saline aquifer (circles), the impedance volume will be used to estimate porosity throughout the survey area.

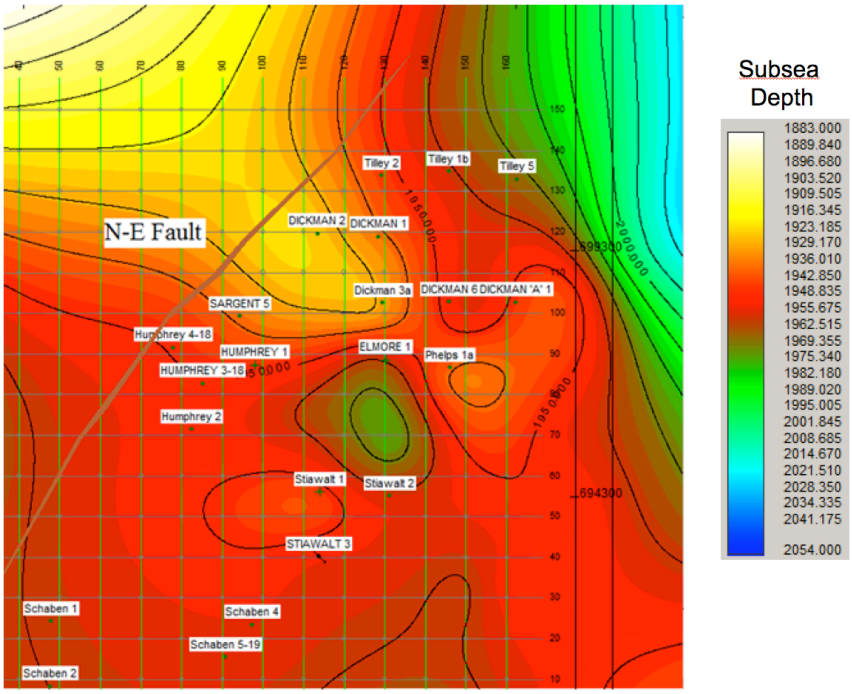

Figure 3-1. Lower Cherokee depth structure map showing location of all 22 production wells and annotated NE bounding fault.

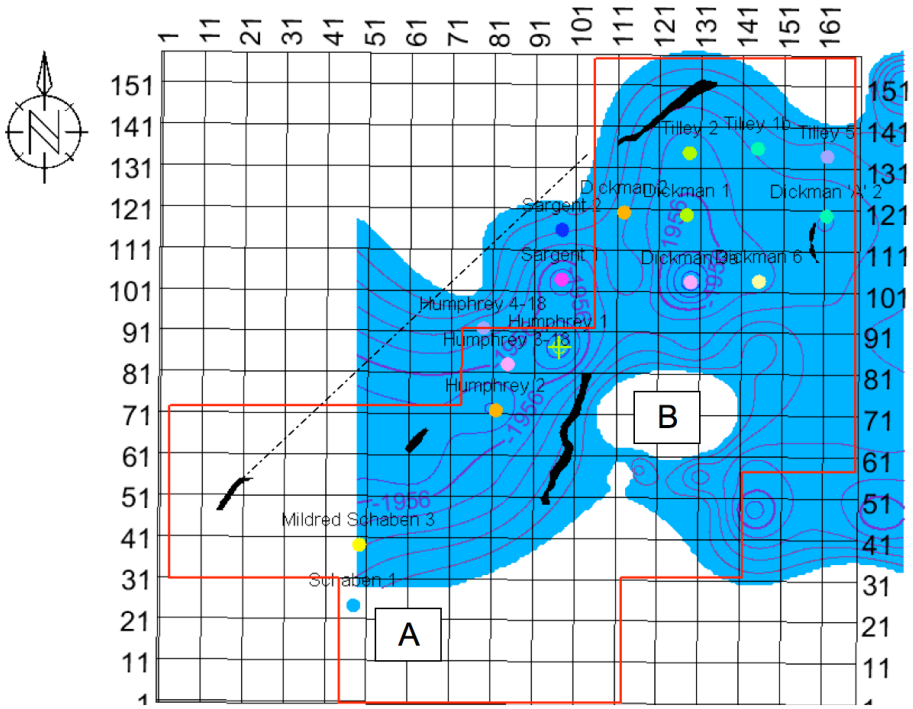

Figure 3-2. Depth structure map of Mississippian Porous carbonate zone above the oil-water contact (-1981 ft TVDSS).

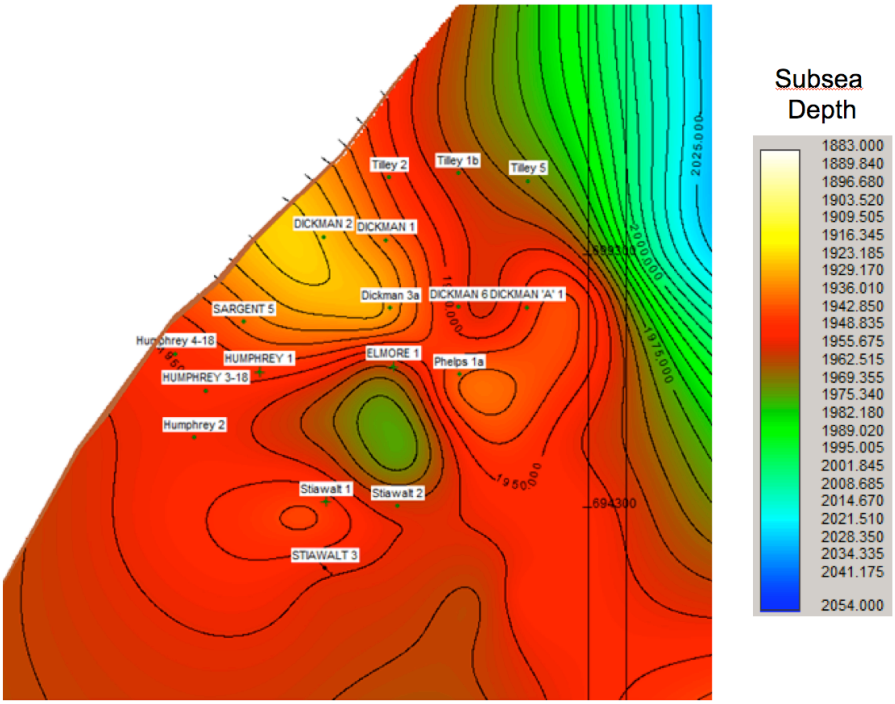

Figure 3-3. Edited top Lower Cherokee depth map. The filed area and production wells will be used for construction of the simulation grid.

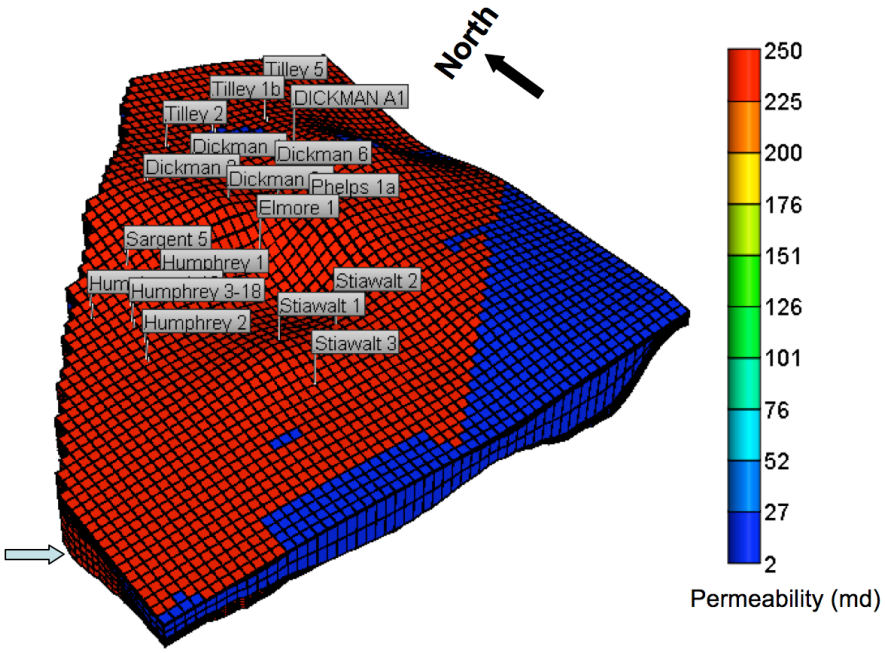

Figure 3-4 Initial simulation grid and the production wells. Arrow indicates the ten layers divided vertically in the grid. The permeability of SE corner has been reduced to 2 md (blue).

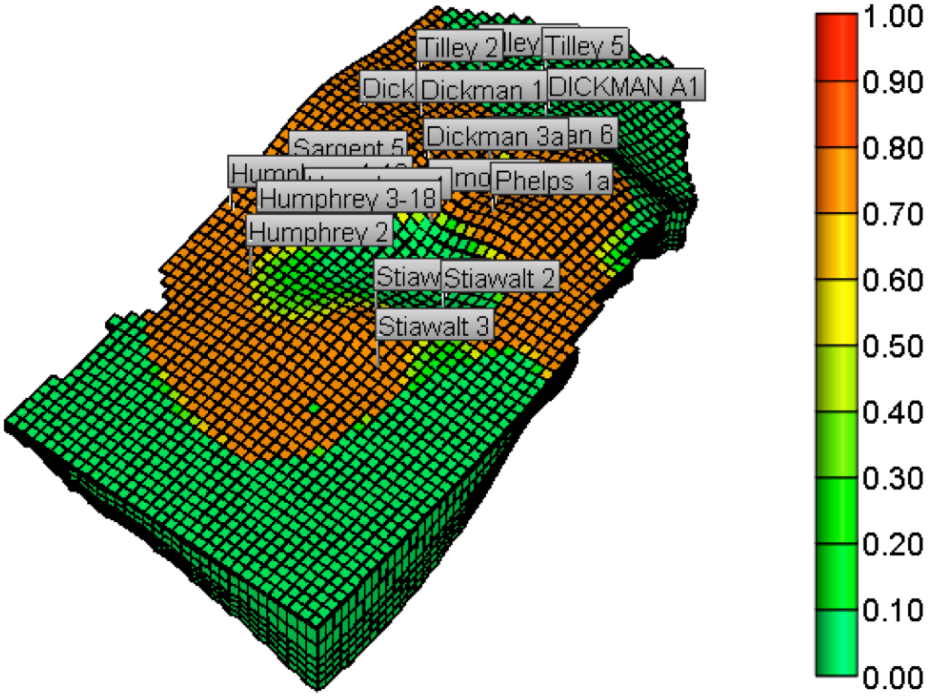

Figure 3-5. Another simulation grid used for history matching. The property shown here is the initial oil saturation.

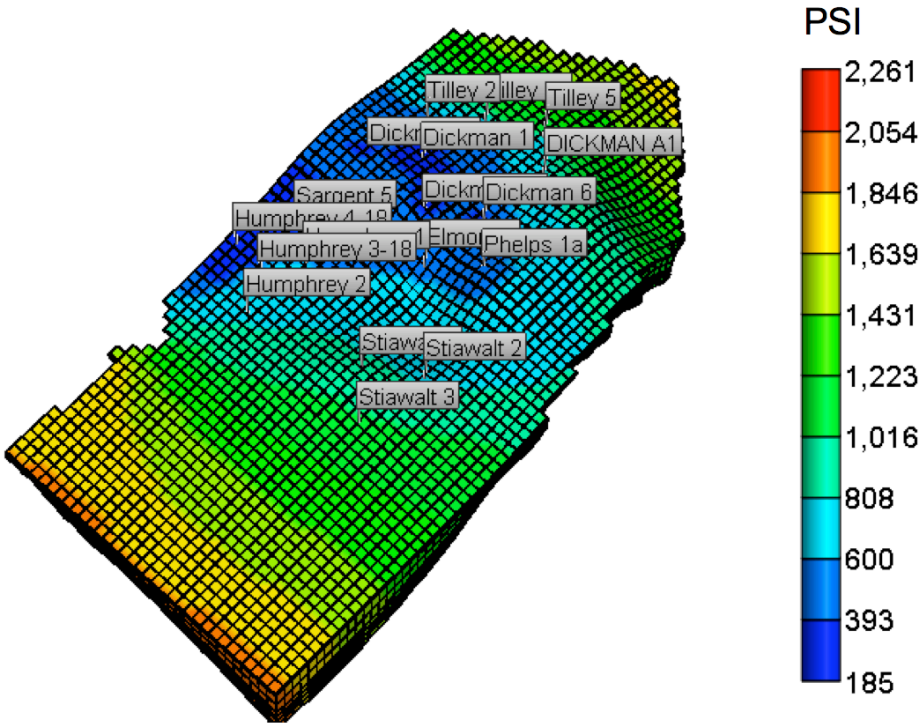

Figure 3-6. Reservoir pressure distribution at the end of simulation

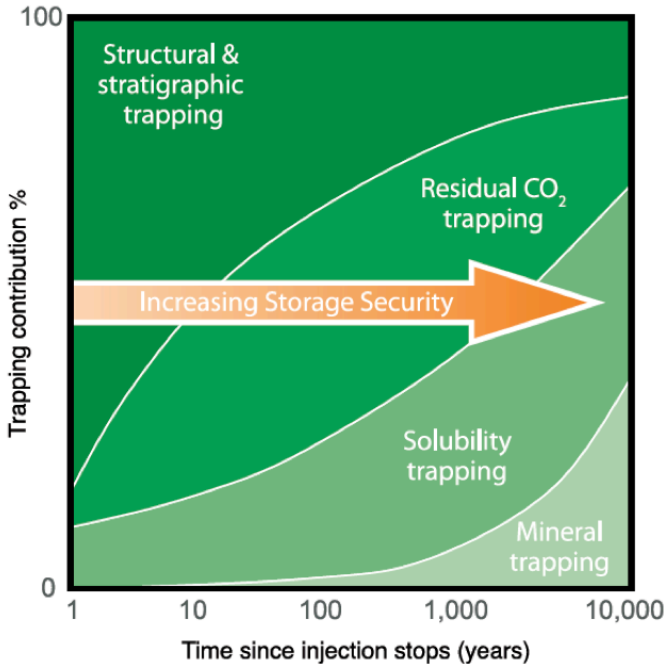

Figure 3-7. CO2 trapping mechanisms as a function of time (from Metz et al, 2005).

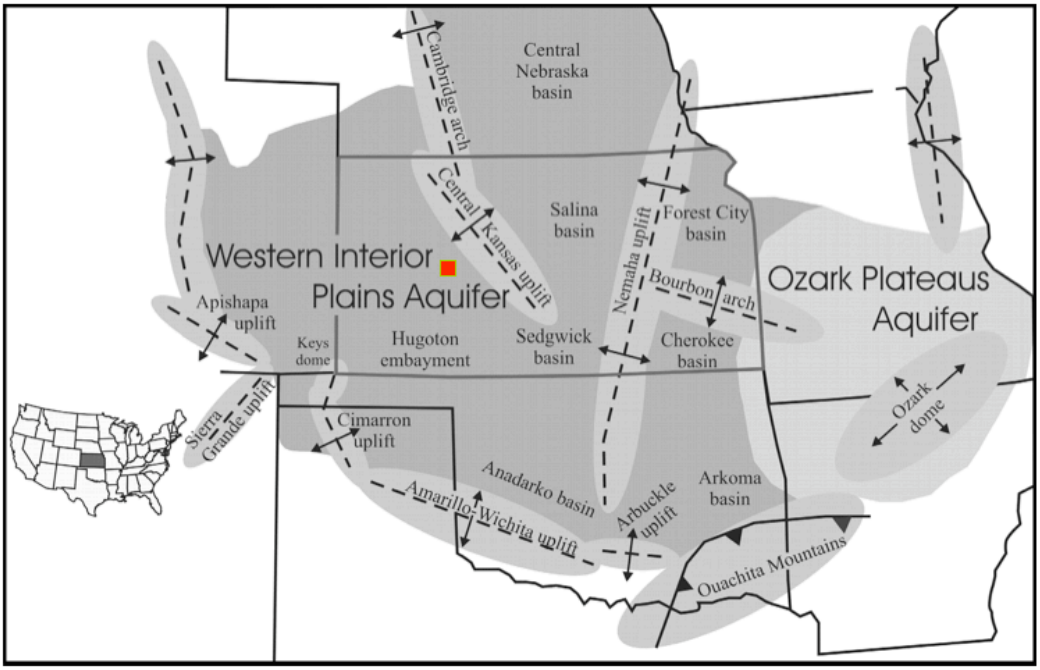

Figure 3-8. Deep saline aquifer system under the state of Kansas (From Carr et al, 2005), with red square indicating location of the Dickman project simulation area.